Ultrathin 2D Fe-nanosheets Stabilized by Mesoporous Silica as Catalysts for Ammonia Synthesis

Hua Fan,[a,b] Jan Markus Folke,[a] Liu Zigeng,[a,e] Frank Girgsdies,[b] Robert Imlau,[d] Holger Ruland, Saskia Heumann,[a] Josef Granwehr,[e,f] Rüdiger-A. Eichel,[e,g] Robert Schlögl,[a,b] Xing Huang,*[,a,b,c] and Elias Frei*[,b]

[a]*Department Heterogeneous Reactions, Max Planck Institute for Chemical Energy Conversion, 45470 Mülheim an der Ruhr, Germany*

[b]*Department of Inorganic Chemistry, Fritz-Haber-Institut der Max-Planck-Gesellschaft, Faradayweg 4-6, 14195 Berlin, Germany*

[c]*Scientific Center for Optical and Electron Microscopy, Otto-Stern-Weg 3, ETH Zurich, 8093 Zurich, Switzerland*

[d]*Thermo Fisher Scientific, Materials & Structural Analysis, Eindhoven, Netherlands*

[e]*Forschungszentrum Jülich, IEK-9, 52425 Jülich, Germany*

[f]*RWTH Aachen University, Institute of Technical and Macromolecular Chemistry, 52074 Aachen, Germany*

[g]*RWTH Aachen University, Institute of Physical Chemistry, 52074 Aachen, Germany*

ABSTRACT

Developing high-performance Fe-based ammonia catalysts through simple and cost-efficient methods has received an increased level of research attention. Herein, we report for the first time the synthesis of two-dimensional (2D) FeOOH nanoflakes encapsulated by mesoporous SiO_2 ($mSiO_2$) *via* a simple solution-based method for ammonia synthesis. Due to the sticking of the $mSiO_2$ coating layers and the limited spaces in between, the Fe after reduction presents 2D morphology, showing high resistance against the sintering during the harsh Haber-Bosch process. Compared to supported Fe nanoparticles dispersed on $mSiO_2$ spheres, the coated catalyst shows a significantly improved catalytic activity by 50% at 425 °C. TDS measurements reveal existence of a higher density of reactive sites for N_2 activation in the 2D Fe catalyst, which are possibly coupled to larger density of surface defect sites (kinks, steps, point defects) that are generally considered as active centers in ammonia synthesis. Besides the structural impact of the coating on the 2D Fe, the electronic one is elucidated by partially substituting Si

with Al in the coating confirmed by ^{29}Si and ^{27}Al MAS NMR. An increased apparent activation energy (E_a) of the Al-containing catalyst evidences an influence on the nature of the active site. The herein developed stable 2D Fe nanostructures can serve as example of a material applied in catalysis offering the chance of a rational catalyst design based on a stepwise introduction of various promoters, in the coating and on the metal, maintaining the spatial control of the active centers.

KEYWORDS: ammonia synthesis, 2D Fe, mesoporous SiO_2, 3D tomography

INTRODUCTION

Catalytic conversion of N_2 and H_2 into NH_3 through Haber-Bosch process is one of the most important inventions in the 20th century. Even after 100 years, we are still relying on this process to sustain adequate food supply for the increasing world population.[1-2] Besides its dominant use in agriculture, ammonia is also an important chemical for manufacturing dyes, plastics and nitric acid, etc.[1, 3-4] Recently, ammonia has been additionally considered as a potential hydrogen carrier due to its high hydrogen density and easy liquefaction for storage and transportation.[5-9]

The industrial catalyst for ammonia synthesis is prepared by melting Fe_3O_4 with different types of promoters (Al_2O_3, CaO and K_2O, etc.) at ca. 2000K.[10] The industrial Haber-Bosch process is carried out typically at high pressure of 150-200 bar and moderately high temperature of 400-500 °C.[11-12] Since both, i.e., catalyst preparation and catalytic reaction, involves the use of dramatic conditions, the energy consumption of them is extremely high. Estimation shows that about 1-2% of global energy is consumed by the industrial Haber-Bosch process each year.[11] It is thus highly desirable to develop simple and cost-economic methods towards synthesis of more efficient catalysts that allows operation at low temperature for ammonia synthesis.[13-14]

Earlier studies have evidenced that the ammonia synthesis is a structure-sensitive reaction.[3, 15-18] Surface sites including kinks, steps and point defects are suggested as the active centers for dissociation of N_2, nearby the NH_3 desorption, identified as rate-limiting step in ammonia synthesis.[19-21] Therefore, to gain a high activity for ammonia synthesis, developing catalysts that contain abundant surface sites is preferential. Another important concern lies in the stability of the active sites during the reaction. Drastic conditions applied in the Haber-Bosch process may result in serious sintering and loss of the active sites.[3] Due to the complex high temperature synthesis of the industrial catalyst, the need for an alternative synthesis approach, enabling a facile control during the catalyst generation, is required.[13-14] Recent progress in the field of two-dimensional (2D) materials have brought unprecedented opportunities for developing novel 2D nanocatalysts for heterogeneous catalysis.[22-25] They

have emerged as important candidates for numerous reactions due to their large surface areas that potentially contain high density of active surface sites.[26-28] In this work, we report for the first time the synthesis of 2D FeOOH nanosheets encapsulated and stabilized by mesoporous SiO_2 ($mSiO_2$) as a precatalyst for ammonia synthesis by a solution-based method. The 2D Fe nanostructures, formed during an *in situ* activation process, are thoroughly characterized by e.g. X-ray diffraction (XRD), N_2 adsorption-desorption analysis, thermo-kinetic methods (TPR and TDS) and electron microscopy. Besides, the structural and electronic impact of the $mSiO_2$ coating is investigated by replacing part of Si with Al. Kinetic investigations are conducted to gain information on the number and nature of the active sites. A special focus is given on the catalyst structure and morphology after testing in ammonia synthesis by high-resolution transmission electron microscopy and 3D tomography.

EXPERIMENTAL SECTION

Chemicals

All chemicals were of analytical grade and used without further treatment. $FeSO_4 \cdot 7H_2O$ and $NaBH_4$ were purchased from Applichem GmbH (Darmstadt, Germany). Cetyltrimethylammonium bromide (CTAB) and tetraethyl orthosilicate (TEOS, 98%) were purchased from Sigma Aldrich. Ammonia solution (25%) was bought from VWR Prolabo. Aluminum isopropoxide ($Al(OiPr)_3$) was purchased from Aldrich Chemicals.

Synthesis of FeOOH nanosheets

The method for the synthesis of ultrathin FeOOH nanosheets has been reported in our previous paper published elsewhere.[29-30] Briefly, 4.2 g $FeSO_4 \cdot 7H_2O$ and 1.8 g CTAB were dissolved in 500 mL distilled water, which was then mixed with 20 mL (4M) freshly prepared $NaBH_4$ solution. After the color turned black, the solution mixture was stirred in open air for 24 h at room temperature. The product was collected by centrifugation, washed with distilled water and ethanol for several times and finally dried at 60 °C.

Synthesis of FeOOH@$mSiO_2$(CTAB)

1 g FeOOH was dispersed in a mixed solution containing CTAB (5 g), distilled water (1 L), ethanol (1 L) and ammonia solution (10 mL). The obtained solution was then stirred at 40 °C for 30 min to produce a uniform dispersion. Next, 3.75 mL TEOS was dropwise added followed by a further stirring for an additional 12 h. The product was collected by centrifugation, washed with distilled water and ethanol for several times and finally dried at 60 °C.

Synthesis of FeOOH@Al/$mSiO_2$(CTAB)

$Al(OiPr)_3$ was used as the Al source in the preparation. The synthesis process is similar to that of FeOOH@$mSiO_2$(CTAB). The only difference is that, 1h after the addition of TEOS, $Al(OiPr)_3$ (170 mg) was introduced to the solution. The nominal Si/Al atomic ratio is 20 in the initial

synthetic solution.

Synthesis of $mSiO_2$(CTAB)

The mixture of distilled water (1 L), ethanol (1 L), CTAB (5 g) and ammonia solution (10 mL) was stirred at 40 °C for 30 min. Afterwards, 3.75 mL TEOS was introduced dropwise into the solution followed by a stirring for 12 h. The product was collected by centrifugation, washed with distilled water and ethanol for several times and dried at 60 °C.

Synthesis of FeOOH/$mSiO_2$(CTAB)

The Fe loading in the above-mentioned coated catalyst (reduced) is estimated to be 38.7 wt%. Similar value is desired in the supported catalyst so that their performance could be fairly compared later. Therefore, 658.2 mg FeOOH and 1.0 g CTAB/$mSiO_2$ were mixed with 500 mL distilled water. The solution was then stirred in the open air at room temperature for 24 h. The product was collected by centrifugation, washed with ethanol and finally dried at 60 °C.

Characterization

The elemental analysis was performed by using an X-ray fluorescence (XRF) of a Bruker P4 engine. Thermogravimetric analysis (TG) was performed by using a Netzsch STA449 Jupiter thermoanalyser. The BET surface area (S_{BET}) was measured by a volumetric N_2-physisorption setup (Autosorb-6B, Quantachrome) at 77 K. Powder X-ray diffraction (XRD) characterization was carried out on a Bruker D8 Advance reflection diffractometer equipped with a Lynx-Eye energy discriminating position sensitive detector (1D-PSD) using Cu-Kα radiation. The magic-angle spinning nuclear magnetic resonance (MAS NMR) measurements were performed on the precatalysts after calcination at 550 °C for 6 h. The calcination process was applied in order to remove the CTAB template and to stabilize the mesoporous (Al/)$mSiO_2$ coating. In addition, the FeOOH nanosheets transform into the corresponding oxide of Fe (Fe_2O_3).[30] The ^{29}Si and ^{27}Al NMR spectra were acquired on a Bruker 800 MHz Avance Neo spectrometer with a 3.2 mm probe at room temperature. The magic angle spinning (MAS) rate is 20 kHz and the pulse sequence is Hahnecho. For ^{29}Si NMR measurement, the 90° pulse and the recycle delay are 5 us and 52 s, respectively. For ^{27}Al NMR acquisition, the 90° pulse and the recycle delay are 2 us and 1 s, respectively. The ^{29}Si shift is referenced to octakis(trimethylsiloxy)silsesquioxane (Q8M8) (11.9 ppm) and the ^{27}Al shift is referenced to 1 M $Al(NO_3)_3$ aqueous solution (0 ppm). Temperature-programmed reduction (TPR) experiments were conducted with 5%H_2/Ar at a flow rate of 80 mL min^{-1} in a fixed-bed reactor. The samples were heated from room-temperature to 700 °C[31] at 6 °C min^{-1} with an isothermal holding period of 90 min. Scanning electron microscopy (SEM) was carried out by Hitachi S-4800 SEM equipped with a field emission gun. Transmission electron microscopy (TEM) was carried out using aberration-corrected JEOL ARM-200CF transmission electron microscope operated at 200 kV. Electron tomography was performed using a Thermo Fisher Scientific Talos F200X operated at 200 kV. The tomographic tilt-series was acquired by scanning transmission

electron microscopy (STEM) using a high-angle annular dark-field (HAADF) detector and a Fischione 2020 tomography holder. Images were recorded every 3° in the tilt range of -64 to +68°. The images of the tilt series were spatially aligned by a cross-correlation algorithm using Inspect 3D software, which was also to reconstruct the 3D volume using a Simultaneous Iterative Reconstruction Technique (SIRT) algorithm. Visualization of the tilt series and 3D volume was performed using Inspect 3D and Avizo software respectively. Thermal desorption spectroscopy (TDS) was applied for the temperature programmed desorption of nitrogen. Therefore, a self-constructed setup which enables the testing of powder samples was used. The setup is equipped with mass flow controllers, an IR-light furnace (BEHR IRF 10) and a mass spectrometer (PFEIFFER VACUUM QME 200). The powder sample is placed on a small quartz-glass boat which is placed in a quartz tube (inner diameter of 14 mm, outer diameter of 20 mm, length of 450 mm) located inside the furnace and connected to the system using Ultra Torr vacuum fittings. Afterwards the system is stepwise brought to $9*10^{-7}$ mbar and directly connected to the mass spectrometer. The reduction at 1bar was carried out at 600 °C for 30 h in a flow of 75% H_2 in N_2. For the nitrogen adsorption at 250 °C, the samples were reduced at 600 °C in 75% H_2 in Ar (again for 30h), cooled to 250 °C and treated for 1h with 75% H_2 in N_2. The TDS measurements were conducted with a heating rate of 25 °C min^{-1}.

Catalytic tests

The catalysts were first pressed into pellets and sieved into grains with size fraction of 250-355 µm. Afterwards, 1g of sieved catalysts (diluted with 1g of SiC) were loaded into a fixed-bed flow reactor and activated *in situ* at 500 °C (1 °C min^{-1}) for 14-16 h in 75% H_2/N_2 (440 NmL min^{-1}). After completion of the reduction, the pressure was raised to 90 bar while the temperature was kept at 500 °C. The total flow rate of 75% H_2/N_2 was adjusted to 200 NmL min^{-1}, keeping the temperature constant for 10 h. Reaction temperatures were varied between 325 and 500 °C in 25 °C steps (1 °C min^{-1}). The produced NH_3 was monitored quantitatively by an IR detector (Emerson X-stream). The apparent activation energies were calculated by using the data in the low-temperature region (below 10% of the thermodynamic equilibrium).

RESULTS AND DISCUSSION

The strategy towards the synthesis of $mSiO_2$ capped 2D Fe catalyst is illustrated in Figure 1a. The starting materials are FeOOH nanosheets which were synthesized *via* a solution-based method as reported in our previous study.[29-30] In the following, we dressed FeOOH nanosheets with a layer of $mSiO_2$(CTAB) composites *via* Stöber-solution growth approach,[32-33] forming a layered core-shell structure (Figure 1a). Note, the CTAB was applied as soft template for mesopores generation in the SiO_2 layer. *In situ* activation (75% H_2/N_2, 500 °C) would eliminate CTAB completely and lead to the formation of mesopores in SiO_2. This process would also give rise to the reduction of FeOOH to metallic Fe. In addition, to discriminate between the morphology of the active Fe moieties and the role of the coating (influence of metal-support interaction), $mSiO_2$(CTAB) spheres supported FeOOH nanosheets and an Al/$mSiO_2$(CTAB) coated FeOOH sample (part of Si substituted by Al) were prepared.

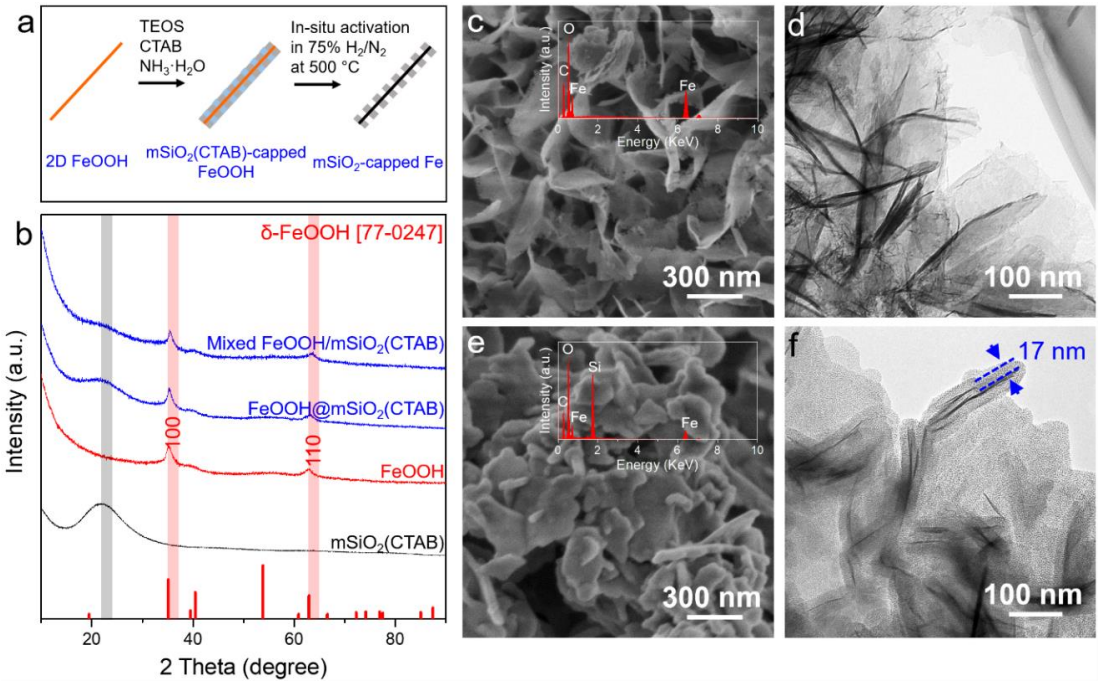

Figure 1. (a) Schematic representation of the fabrication process for 2D core-shell Fe@mSiO_2 catalyst; (b) XRD patterns of mSiO_2(CTAB) spheres and the as-prepared FeOOH nanosheet-based precatalysts; (c,e) SEM images of FeOOH nanosheets and mSiO_2(CTAB) capped FeOOH, respectively; (d,f) TEM images corresponding to (c,e).

The composition of the as-prepared samples was analyzed quantitatively by combination of X-ray fluorescence (XRF) and thermogravimetric analysis (TG) (see Figure S1). The results are listed in Table 1. The loading amount of Fe in the coated sample is measured as 24.3 wt% while a similar value (25.5 wt%) is determined for the supported one. Since both samples show a SiO_2/CTAB mass ratio of 1.7, one can expect that after removal of CTAB during the activation process, the total Fe loading should be close (ca. 38.7% and 40.4% for coated and supported samples). The sample with Al dopant contains slightly less Fe (21.9 wt%) in the precursor state and after activation, it is expected to be ca. 34.7 wt%. The corresponding Si/Al atomic ratio is 20.6, consistent with its nominal value.

Table 1. Physical properties of the as-prepared catalysts.

Sample	Fe loading (wt%)		SiO_2:CTAB mass ratio	S_{BET} (m^2/g)
	Catalyst	Precursor		
$mSiO_2$(CTAB)	–	–	1.9	18.7
$mSiO_2$	–	–	–	900.5
FeOOH nanosheets	100	62.9	–	151.6
FeOOH@$mSiO_2$(CTAB)	38.7	24.3	1.7	80.1
FeOOH@Al/$mSiO_2$(CTAB)	34.6	21.9	1.7	63.6
Mixed FeOOH/SiO_2(CTAB)	40.4	25.5	1.7	116.6

The pore structures of samples were characterized by N_2 adsorption-desorption analysis (Table 1 and Figure S2). As displayed in Table 1, the surface areas of $mSiO_2$(CTAB) and FeOOH nanosheets are 18.7 and 151.6 m^2/g, respectively. After the introduction of $mSiO_2$(CTAB) (or Al/$mSiO_2$(CTAB)) as either the coating or support materials, the derived samples show smaller surface areas (80.1 m^2/g for FeOOH@$mSiO_2$(CTAB), 116.6 m^2/g for mixed FeOOH/SiO_2(CTAB) and 63.3 m^2/g for FeOOH@Al/$mSiO_2$(CTAB)) compared to FeOOH nanosheets. This is due to the fact that mesopores of $mSiO_2$ are still blocked by CTAB. After calcination, removal of CTAB leads to dramatically increased surface area of $mSiO_2$ from 18.7 to 900.5 m^2/g with an average pore size of ca. 2 nm (Figure S2b). The porous structure of $mSiO_2$ is stable under harsh Haber-Bosch process, which is verified by the still remaining large surface area (800 m^2/g) and narrow pore size (ca. 4 nm) of the spent catalyst.

Electron microscopy and X-ray diffraction (XRD) were further employed to characterize the as-prepared precursors. The scanning electron microscopy (SEM) image in Figure 1c clearly reveals that the FeOOH displays a flexible and mildly curved 2D structure. The semi-transparency feature characterized by bright-field transmission electron microscopy (BF-TEM) suggests that the FeOOH nanosheets are very thin, and according to high-resolution TEM (HRTEM) image shown in Figure S3, the FeOOH sheet thickness is about 2-4 nm. Structural analysis based on the XRD further reveals that the obtained FeOOH nanosheets crystallize as δ-FeOOH phase (ICDD PDF-2 77-0247). The reflections locating at 35° and 63° (2θ) can be assigned to 100 and 110 planes of δ-FeOOH (Figure 1b).[34]

After the coating process, the FeOOH@$mSiO_2$(CTAB) shows an increased thickness, as evidenced in Figure 1e. The energy dispersed X-ray spectroscopy (EDX) spectrum shown in the inset of Figure 1e reveals a significant presence of Si signal (compared to Figure 1c). This confirms the successful coating of the SiO_2 layer on FeOOH nanosheets. The XRD pattern of

the coated sample shows an additional peak at 22°, which can be due to the presence of amorphous SiO_2.[35] ^{29}Si MAS NMR spectrum of the calcined precatayst Fe_2O_3@$mSiO_2$ in Figure S4 indicates the presence of two Si species with different coordination environments. The peaks at chemical shifts of -110.9 and -100.0 ppm are due to the Si sites in $Si(OSi)_4$ (Q^4, 57.4 %) and $Si(OSi)_3$-OH (Q^3, 42.6 %), respectively.[36] The former Si species locates in the interior part of the SiO_2 coating, while the later one stays on the coating surface.[36] In good agreement with the high surface area of $mSiO_2$, the amount of the surface Si species is nearly as high as half of the total Si species. To study the thickness of the coating layer, TEM was further performed. As shown in Figure 1f, the cross-section view of nanosheets reveals about 17 nm of the SiO_2 layers. As the FeOOH nanosheets are fully covered by SiO_2 layers and the spaces between layers are constrained, we expect the 2D structured Fe to form during the activation process. Since the activation was done *in situ* in the reactor, and after the activation process, the catalyst was tested directly under ammonia synthesis condition, the activated sample is not available for characterizations. Nevertheless, the formation of mesopores in SiO_2 is evidenced for the spent catalyst, suggesting that activation process can efficiently remove the CTAB from pores of SiO_2.

The XRD measurement of the supported sample (Figure 1b) shows reflections from both FeOOH and SiO_2, which are very similar to that of the coated precursor. The $mSiO_2$(CTAB) spheres alone (Figure S5a) shows relative smooth surfaces with a diameter mostly in the range from 650 nm to 1 µm. After mixing with FeOOH, the surface of spheres become rather rough, considerably due to the coverage by FeOOH sheets (Figure S5b). The elemental maps of the coated and supported samples are shown in Figure S6. One can see that the distribution of Fe and Si in the coated sample is apparently more homogeneous than that in the supported one. TEM images of the supported sample (Figure S5c,d) indicate that FeOOH nanosheets and SiO_2 spheres are not uniformly mixed.

The introduction of Al dopant caused no obvious change in the XRD pattern of the coated sample (Figure S7). EDX measurement (Figure S8) confirm the presence of Al as part of the coating which is distributed homogeneously. To investigate the coordination environment of Al within the coating, ^{29}Si and ^{27}Al MAS NMR investigations were performed on the calcined precatalyst Fe_2O_3@Al/$mSiO_2$ (Figure S9). The signals at 9.8 ppm and 58.4 ppm in the ^{27}Al spectrum correspond to the six-coordinated and four coordinated Al species, respectively.[37] This result evidences that a significant amount of Al was successfully incorporated into the SiO_2 framework and formed Al-O-Si bonds at the expense of Q^4 sites, which is further confirmed by the ^{29}Si spectrum.[37] This guarantees a direct attachment of Al to the 2D Fe structures as part of the oxide coating and enables investigations on the role of metal-support interactions.

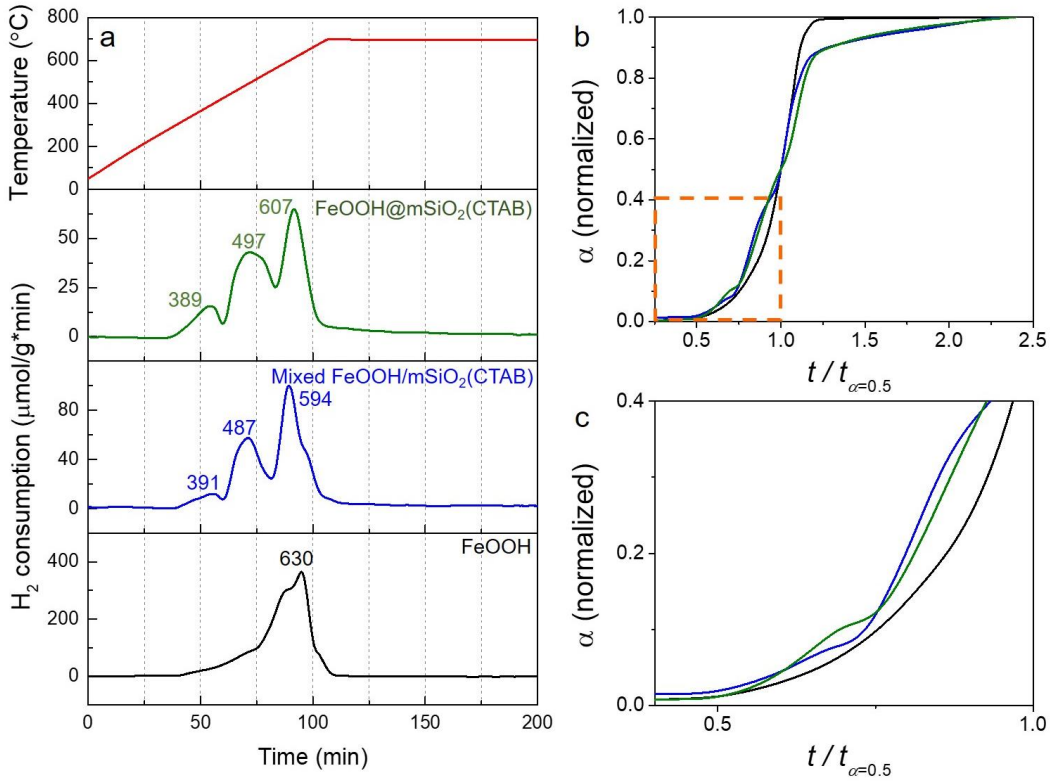

Figure 2. (a) H_2-TPR of FeOOH (black), $mSiO_2$ supported (blue) or coated (green) FeOOH; (b) Integrated TPR curves to time-fractions ($t/t_{\alpha=0.5}$); (c) Zoom-in of the selected area indicated in (b). Conditions: 5%H_2/Ar, 80 mL min^{-1}, 6 °C min^{-1}, 700 °C, 90 min holding time.

To investigate the reduction behaviors of the catalyst precursors, temperature-programmed reduction (TPR) analysis was carried out by ramping the temperature to 700 °C at a heating rate of 6°C min^{-1} in 5%H_2/Ar. The Al-containing sample shows an almost identical reduction behavior with the SiO_2 coated sample and therefore is not separately discussed (See Figure S10). One can see that both, the FeOOH@$mSiO_2$(CTAB) and the mixed FeOOH/$mSiO_2$(CTAB), show a similar reduction behavior with the presence of three main peaks located at around 390, 490 and 600 °C, respectively (see Figure 2a). Since almost no H_2 consumption is observed for the $mSiO_2$(CTAB) (see Figure S11), the consumption peaks observed from both precursors can be solely attributed to the reduction of FeOOH. Additionally, occurrence of reduction in the coated sample implies that the CTAB in pores of SiO_2 layers can be fully removed during the reduction process so that it will not inhibit the reduction of the coated FeOOH. Generally, FeOOH follows a three-step reduction at elevated temperature following the path: FeOOH → Fe_3O_4 → FeO → Fe.[30, 38] The presented three consumption peaks most likely response to the reduction processes from FeOOH → Fe_3O_4, Fe_3O_4 → FeO, and FeO → Fe, respectively. However, for unsupported FeOOH nanosheets,

the different steps are not well resolved. The maximum H_2 consumption appears at 630 °C, which is ca. 30 °C higher compared to that for the SiO_2-containing catalysts. The shift to higher reduction temperature is considerably attributed to the aggregation of the nanosheets due to the lack of support materials. It needs to be mentioned that the calculated H_2 consumption amount is still much less than the total amount needed for the full reduction, suggesting that the partial samples are not fully reduced under the applied condition. The reduction degrees for FeOOH, FeOOH@mSiO_2(CTAB), FeOOH/mSiO_2(CTAB) and FeOOH@Al/mSiO_2(CTAB) are 58%, 37%, 37% and 38%, respectively. In order to gain more insights on the reduction mechanism, independent of a temperature shift, the integrated TPR profiles are normalized to time-fractions ($t/t_{\alpha=0.5}$), as shown in Figure 2b,c as α-plots. One can see that the α-plots of encapsulated FeOOH and supported FeOOH show close shape and inclination, indicating a similar reduction mechanism. There are still some minor differences existed, for example, the shift in shoulder position ($t/t_{\alpha=0.5}$=0.62-0.75), which could be due to the slightly different contact area between metal and SiO_2. The coated sample, in comparison to the supported one, shows a faster reduction of the first event and a slower and lasting reduction of the following steps. In contrast, the α-plot of unsupported FeOOH nanosheets shows a sharper inclination and shifts towards higher $t/t_{\alpha=0.5}$, suggesting a different reduction mechanism. Beyond 0.5 of the integrated area, the α-plots give information on the autocatalytic character of the reduction process. The pure Fe sample curve increases strongly, indicative for a support and dispersion free reduction with strong autocatalytic contribution. This strong autocatalytic character of the reduction process beyond 0.5 t/t_{α} values explains the higher degree of reduction for FeOOH (58%). The SiO_2-containing samples show a small autocatalytic contribution due to the high dispersion.

In summary, the set of samples (supported, coated, coated with Al dopant), investigated with respect to their structural and physico-chemical properties, show only small variations attributed to the intended changes of the morphology (insignificant difference in reduction behavior, slightly less dispersed) and coating (almost identical). Hence, they are perfectly suitable for the analysis of their catalytic performances.

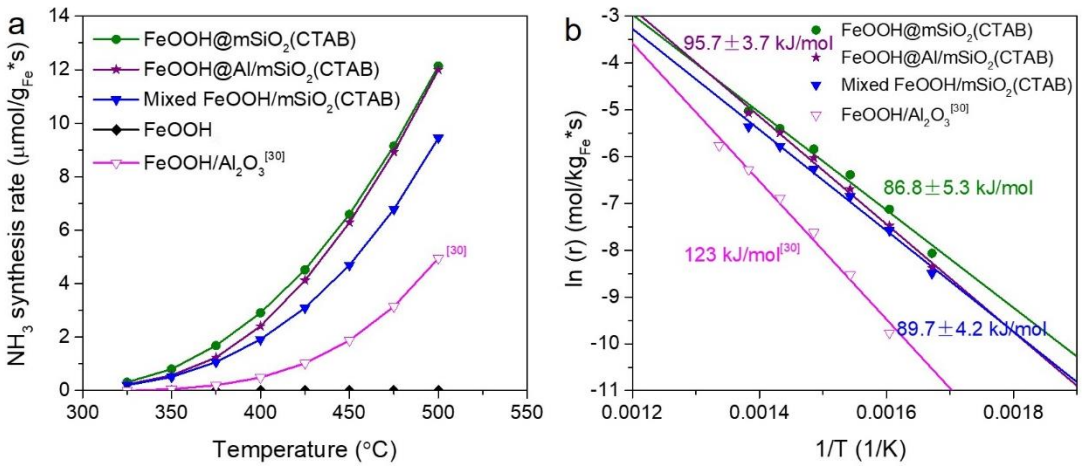

Figure 3. (a) Fe mass normalized NH_3 production rates. (b) Arrhenius plots for NH_3 synthesis at 90 bar over the γ-Al_2O_3 supported[30] (pink), $mSiO_2$ supported (blue) and coated (without Al: green, with Al: purple) catalysts. Reaction conditions: 75%H_2/N_2, 200 NmL min^{-1}, 90 bar.

In situ catalytic activation was performed on the precursors in 75% H_2/N_2 at 3-4 bar with a heating rate of 1°C min^{-1} up to 500 °C. The MS data shows the formation of water prior to the onset of ammonia in SiO_2 coated (with and without Al) and supported catalysts, whereas for unsupported FeOOH there is no ammonia detected. (Figure S12). The water signal generated at around 100 °C is mainly from the surface adsorbed water and that appeared at high temperatures is due to the reduction of catalysts. In comparison with the TPR experiments that show distinguished water peaks due to different steps of reduction, serious overlapping of water peaks is observed on samples during activation process, which is considerably due to the much slower heating rate of the activation. It is also noted that the coated and supported samples show the cease of water formation in slightly longer time than the unsupported sample, indicating a delayed reduction. This result indeed agrees well with the TPR measurements.

In preparation for the subsequent activity test, the pressure was then elevated to 90 bar and kept for 10 h at 500 °C. It is found that during this period the SiO_2 supported sample shows a significant deactivation before getting stabilized (Figure S13b). However, a further increased activity is observed for the coated sample (Figure S13a,c). We propose that the reduced activity in the supported sample might be due to an increased degree of sintering induced by the pressure increase, in particular $p(H_2)$, that leads to the loss of active surfaces. Furthermore, the reaction temperature is varied stepwise from 500 °C to 325 °C with a 25 °C interval and back again to 500°C. We find that the SiO_2 coated samples are more active than the SiO_2 supported one in the steady-state (see Figure S13). At 425 °C, the NH_3 production rate of the SiO_2 coated FeOOH sample amounts to 4.5 μmol g_{Fe}^{-1} s^{-1}, which is ≈50% more active than that of the SiO_2 supported one (3.1 μmol g_{Fe}^{-1} s^{-1}) (see Figure 3a). Interestingly,

despite that the reaction rate of the coated and supported catalysts is different, the apparent activation energy is very close in both cases (Figure 3b). This result implies that the two catalysts with the same support material contain the same type of active species (and likely a similar metal-support interaction). It is suggested that the activity difference is defined by the number of active sites (higher dispersion), in line with the α-plot profile. When Al was incorporated into the coated catalyst, the reaction rate is slightly decreased to 4.1 μmol g_{Fe}^{-1} s^{-1}. However, the corresponding apparent activation energy is elevated from 86.8 kJ mol^{-1} to 95.7 kJ mol^{-1} (ca. 10% higher), indicating an influence on the nature of the active sites. In general, SiO_2 is regarded as one of the most used inert support for numerous catalysts[39-40] and a standard structural promoter for industrial ammonia synthesis catalysts[3]. However, in the current catalysts, it seems that the $mSiO_2$ coating is more than a structural stabilizer and electronic effects likely occur. In other words, the different interaction of Fe and the corresponding support materials ($mSiO_2$ and $Al/mSiO_2$) might lead to another interfacial (metal-oxide) contact and consequently to a change of the local Fe structure, and respectively active site. These findings agree well with our previous research results, where the catalytic performance of a *γ*-Al_2O_3 supported FeOOH nanosheet catalysts were explained by the density of kinks and steps within the active Fe structures (see also Figure 3, $FeOOH/Al_2O_3$ performance as reference).[30] Obviously, SiO_2, either as a support or a coating material, is a better support than *γ*-Al_2O_3 for the FeOOH nanosheets. This might be explained by the interfacial formation of Fe-silicide[41] structures acting as intrinsic stable structural (more defects) and electronic (different active sites) promoters. The stability of such interaction is confirmed by isothermal testing of catalysts at 425 °C and 90 bar for more than 45 h. All of the SiO_2 involved catalysts show long-term durability with a negligible loss of activity (Figure S14).

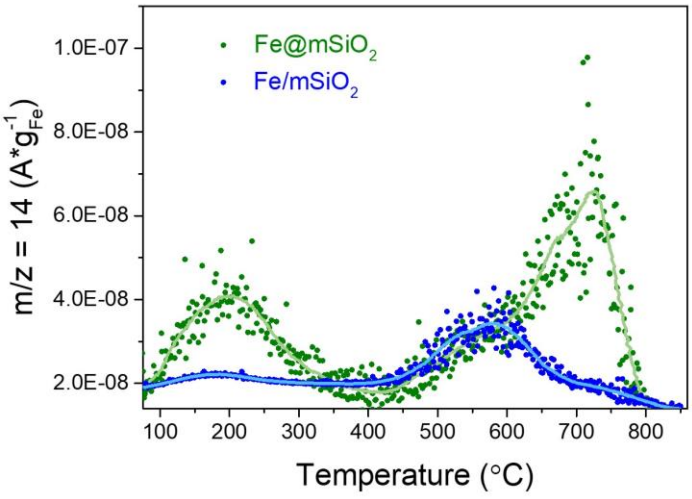

Figure 4. TDS spectra of the $mSiO_2$ supported and coated Fe catalysts. The samples were activated under 1 bar in a flow of 75%H_2/N_2 at 600 °C for 30 h. The TDS measurements were

conducted with a heating rate of 25 °C min^{-1}. The solid curves are smoothed data to guide the eye.

To have access to different kinds of surface sites N_2-TDS measurements were performed on the coated and supported Fe nanostructures. Figure 4 shows the TDS signal of the m/z=14 with respect to the Fe mass. Prior to the desorption experiment, the samples were activated *in situ* for 30 h at 600 °C under a flow of 75%H_2/N_2. The TDS signals differ significantly in two regions, a low temperature desorption event at around 200 °C and a high temperature one at 700 °C. A common event is observed at 550 °C. The low temperature desorption is attributed to weakly bound N-species. This might be related to interfacial Fe sites (Fe-mSiO_2 interface), highly populated in the mSiO_2 coated system. The common event is likely attributed to defect sites like kinks and steps/step edges, which are generally seen as active centers for the ammonia synthesis.[21] The late desorption event of the coated sample is related to N-reconstruction of terrace sites, possibly related the additional formation of subsurface Fe-N species (indicated by the signal drop observed for desorption events zero order). Another TDS experiment shown in Figure S16a of the mSiO_2 coated catalyst highlights the ability of the 2D nanostructures to activate N_2 at moderate temperatures of 250 °C (reduction in 75%H_2/Ar at 600 °C for ca. 30 h and a subsequent H_2/N_2 treatment at 250 °C for 1 h). The high temperature events are significantly reduced (at 700 °C) or absent (at 550 °C). This means the terrace reconstructions and subsurface N-species are interpreted as a coverage/poisoning of the Fe surface, also formed under the harsh conditions of the ammonia synthesis. This phenomenon is significantly decreased for the mSiO_2 supported catalyst. The interfacial Fe sites, responsible for the low temperature desorption event, are, however, still completely recovered. As reference experiment on the role of the support (and the interfacial Fe contact), the Al_2O_3 supported Fe catalysts, which has shown a lower activity and increased apparent activation energy is analyzed with TDS (Figure S16b). The low temperature desorption event is absent, the defect related one is shifted by ca. 50°C towards higher temperatures and the reconstructions are rather pronounced. This might explain the poor catalytic performance in comparison to the SiO_2 samples. A fully promoted industrial catalyst, still much more active than the unpromoted SiO_2 systems, shows only one desorption event (Figure S16c). The signal likely related to defect sites (also promoter induced) are shifted by 50 °C to lower temperatures, exactly the temperature relevant for the industrially applied ammonia synthesis. The industrial reference catalyst, however, is not able to activate N_2 at 250 °C, but the set of added promoters shift the defects sites to lower temperatures and avoids any surface poisoning by reconstructions (no high temperature desorption). To sum up, the 2D Fe structures stabilized by mSiO_2 shows the ability to activate N_2 at moderate temperatures (one important criterion for high reaction rates), but on the other hand tends to N-induced poisoning

effects, which might be coupled to a strong binding of the NH_3 product (as another rate determining criterion, absent in the industrial catalyst). This means, a promoter optimized 2D Fe catalyst might combine the positive effects of low temperature N_2 activation, low temperature defect sites without N-reconstructions, as part of a separated study.

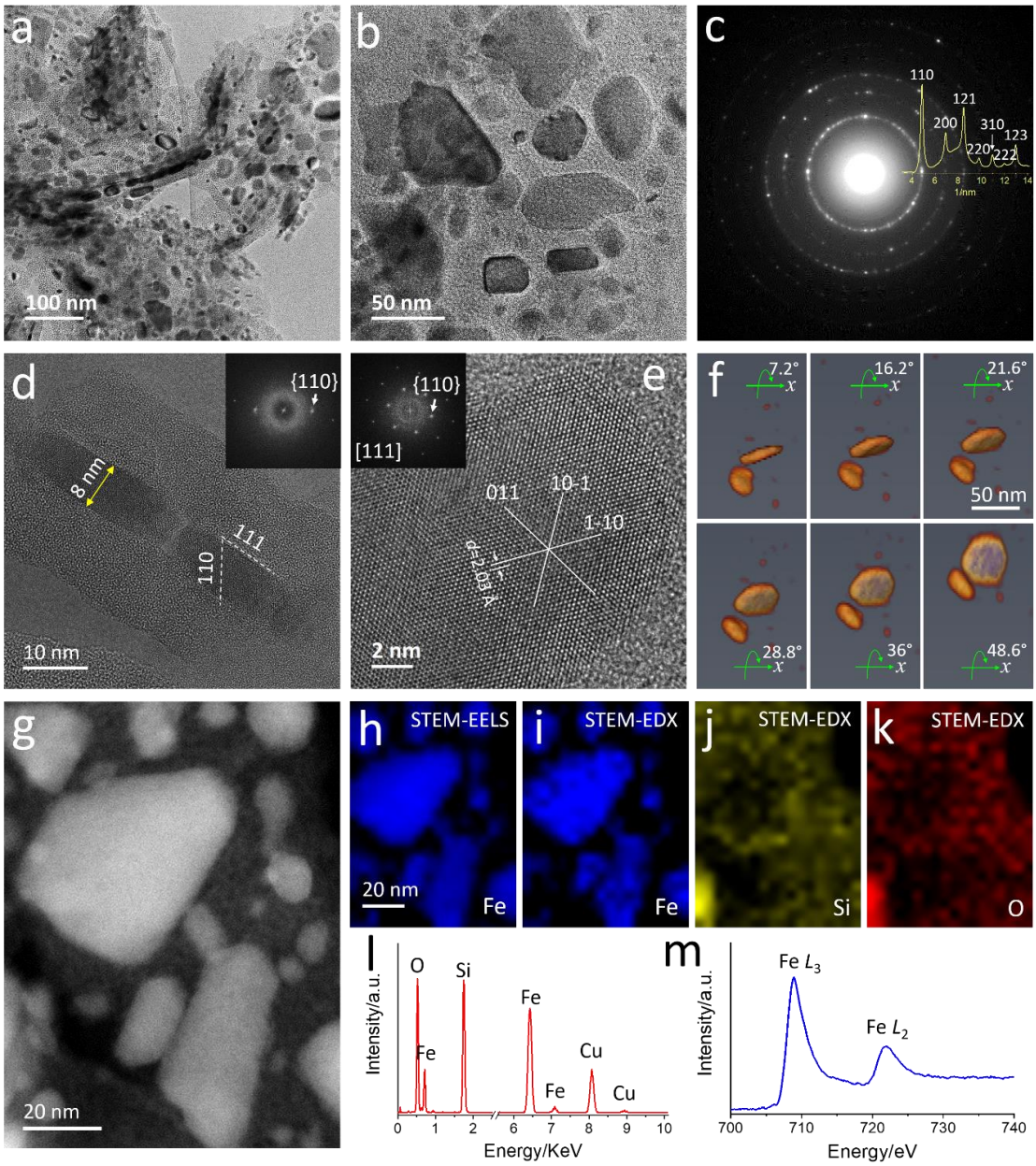

Figure 5. (a,b) TEM images and (c) selective-area electron diffraction of spent coated catalyst; (d,e) HRTEM images of cross-section view and plane view of catalyst, revealing 111 orientated Fe nanoplates; (f) 3D tomography of catalyst, confirming the formation of 2D Fe; (g) HAADF-STEM image and (h, j-l) elemental analysis of coated catalysts; (i) STEM-EELS map of Fe and (m) corresponding EELS spectrum. Note: there was no air contact during the sample transfer from the reaction tube into the chamber of TEM.

In order to gain insights about the maintained morphology, structure and composition of SiO_2 coated catalyst (as prerequisite for any optimization approaches), the spent sample was comprehensively characterized by XRD, TEM in combination of EDX and EELS techniques. Figure 5a shows a typical low magnification BF-TEM image of Fe@mSiO_2 core-shell structure after a series of catalytic tests. The TEM image recorded at higher magnification is shown in Figure 5b. Unlike the precursor catalyst that shows continuous sheet-like structure with a relative weak contrast under the coating layer, the spent catalyst shows the clear presence of nanoparticles with the size ranging from a few to several tens of nanometer. Closer observations further reveal that most of the nanoparticles likely have a 2D morphology (Figure 5b). Based on the secondary electron (SE) image recorded simultaneously with BF-STEM and HAADF-STEM images shown in Figure S17, the nanoparticles are still embedded into the SiO_2 layers. The diameter of the mesopores in the SiO_2 layer is measured as 1.5-4 nm, as shown in Figure 5b and Figure S18, perfectly in line with the pore distribution determined by N_2 adsorption isotherms. To reveal the phase of the activated catalyst, selective-area electron diffraction (SAED) was taken (Figure 5c), which assuredly demonstrates the formation of metallic Fe in a bcc structure. It is also confirmed by the XRD analysis of the spent catalyst (see Figure S20). The 2D structure of Fe is further highlighted by cross-section view high-resolution TEM (HRTEM) image shown in Figure 5d which reveals the thickness of Fe plates of ca. 8 nm. According to the structural analysis, the top/bottom surfaces are enclosed with 111 facets. Figure 5e shows a plan-view HRTEM image of a nanoplate orientated along the 111 direction. The lattice fringes with a d-spacing of 2.03 Å fit well to the 110 planes of bcc Fe. In order to further confirm the 2D structure of the Fe, the electron tomography, a method to construct 3D information from serial 2D images, is employed to examine the morphology of Fe. The procedure for data acquisition is provided in the experimental section. As shown in Figure 5f, a series of images with different rotation angle along x-axis clearly demonstrate the 2D morphology of Fe particles. A larger view with more particles present is provided in Movie 2. We also performed the compositional analysis using STEM-EDX. The elemental mapping reveals the distribution of Fe that is surrounded by Si and O (Figure 5i-k). To confirm the metallic phase of Fe from an electronic structure point of view, the STEM-EELS spectrum and map were spontaneously recorded with the EDX analysis. The EELS map (Figure 5h) shows a similar distribution of Fe compared to that determined by EDX map. Moreover, analysis of Fe $L_{2,3}$-edges about the chemical position and feature of spectrum fit well to the metallic Fe of the catalyst.[42-43]

Comparing to the coated catalyst, the particle dispersion in the supported spent catalyst is obviously less homogeneous (Figure S19a). Agglomeration of nanoparticles is also found. Interestingly, there are a portion of particles also appearing in 2D shape, which is probably inherited from the initial 2D morphology of the FeOOH. The electron diffraction (inset of Figure

S19a) evidences that the Fe particles are in metallic phase, which is in agreement with the XRD result (see Figure S20). The HRTEM image of an 001 orientated Fe nanoparticle shows lattice d-spacing of 2.04 Å, corresponding to 110 planes of bcc Fe (Figure S19b). In contrast to the SiO_2 coated or supported catalysts that contains small nanoparticles, the unsupported catalyst (Figure S21) shows much larger particle size (several tens to hundreds nm). The particles have quite smooth surfaces terminated mostly with 100 and 110 planes. An increased trend of Fe size is also revealed by the XRD analysis (Figure S20). For the coated and supported catalysts, the domain size is estimated to be 14 nm (15 nm for the Al-containing catalyst) and 19 nm, respectively. However, for unsupported one, the size increases profoundly to 87 nm. The serious sintering and agglomeration of catalytic particles result in the significant loss of active sites, thus presenting a negligible activity. As for the higher activity observed from the coated catalysts compared to the supported one, our experimental evidences point to the origin of formation of 2D structures, which provides a higher density of kinks/steps and interfacial sites relevant for the for N_2 dissociation and NH_3 formation.

CONCLUSION

In summary, we report the fabrication of SiO_2 encapsulated FeOOH nanosheets as a catalyst precursor for ammonia synthesis through a facile and low-cost solution-based method. TEM characterization of catalyst performed after *in situ* activation and a series of catalytic tests implies that the catalyst on work contains 2D Fe nanostructures embedded into porous SiO_2 layers. The 2D Fe catalyst shows a higher catalytic activity compared to the supported catalyst containing Fe nanoparticles supported on the SiO_2 spheres (1.5 times higher at 425 °C). Although the two catalysts present different activity, they show very close activation energy, indicating the same types of active species. The catalyst with Al-doped $mSiO_2$ (FeOOH@Al/$mSiO_2$) shows slightly lower activity yet higher activation energy than the non-doped catalyst (FeOOH@/$mSiO_2$), suggesting that Al doping introduces a structural and electronic effect that changes the nature of active site negatively. In consideration of our experimental results based on mutual characterization techniques, we propose that the higher activity of the encapsulated catalyst is attributed to the formation of 2D Fe nanostructures that can expose more active surface sites compared to the supported Fe nanoparticles. The herein presented synthetic method could serve as an experimental basis for rational design and economic synthesis of efficient 2D Fe-based catalysts for ammonia synthesis upon adding dedicated promoters.

Supporting Information

Mesoporous Silica Encapsulated Ultrathin 2D Iron for Ammonia Synthesis

Hua Fan,[a,b] Jan Markus Folke,[a] Liu Zigeng,[a,e] Frank Girgsdies,[b] Robert Imlau,[d] Holger Ruland, Saskia Heumann,[a] Josef Granwehr,[e,f] Rüdiger-A. Eichel,[e,g] Robert Schlögl,[a,b] Xing Huang,*[,a,b,c] and Elias Frei*[,b]

[a]*Department Heterogeneous Reactions, Max Planck Institute for Chemical Energy Conversion, 45470 Mülheim an der Ruhr, Germany*

[b]*Department of Inorganic Chemistry, Fritz-Haber-Institut der Max-Planck-Gesellschaft, Faradayweg 4-6, 14195 Berlin, Germany*

[c]*Scientific Center for Optical and Electron Microscopy, Otto-Stern-Weg 3, ETH Zurich, 8093 Zurich, Switzerland*

[d]*Thermo Fisher Scientific, Materials & Structural Analysis, Eindhoven, Netherlands*

[e]*Forschungszentrum Jülich, IEK-9, 52425 Jülich, Germany*

[f]*RWTH Aachen University, Institute of Technical and Macromolecular Chemistry, 52074 Aachen, Germany*

[g]*RWTH Aachen University, Institute of Physical Chemistry, 52074 Aachen, Germany*

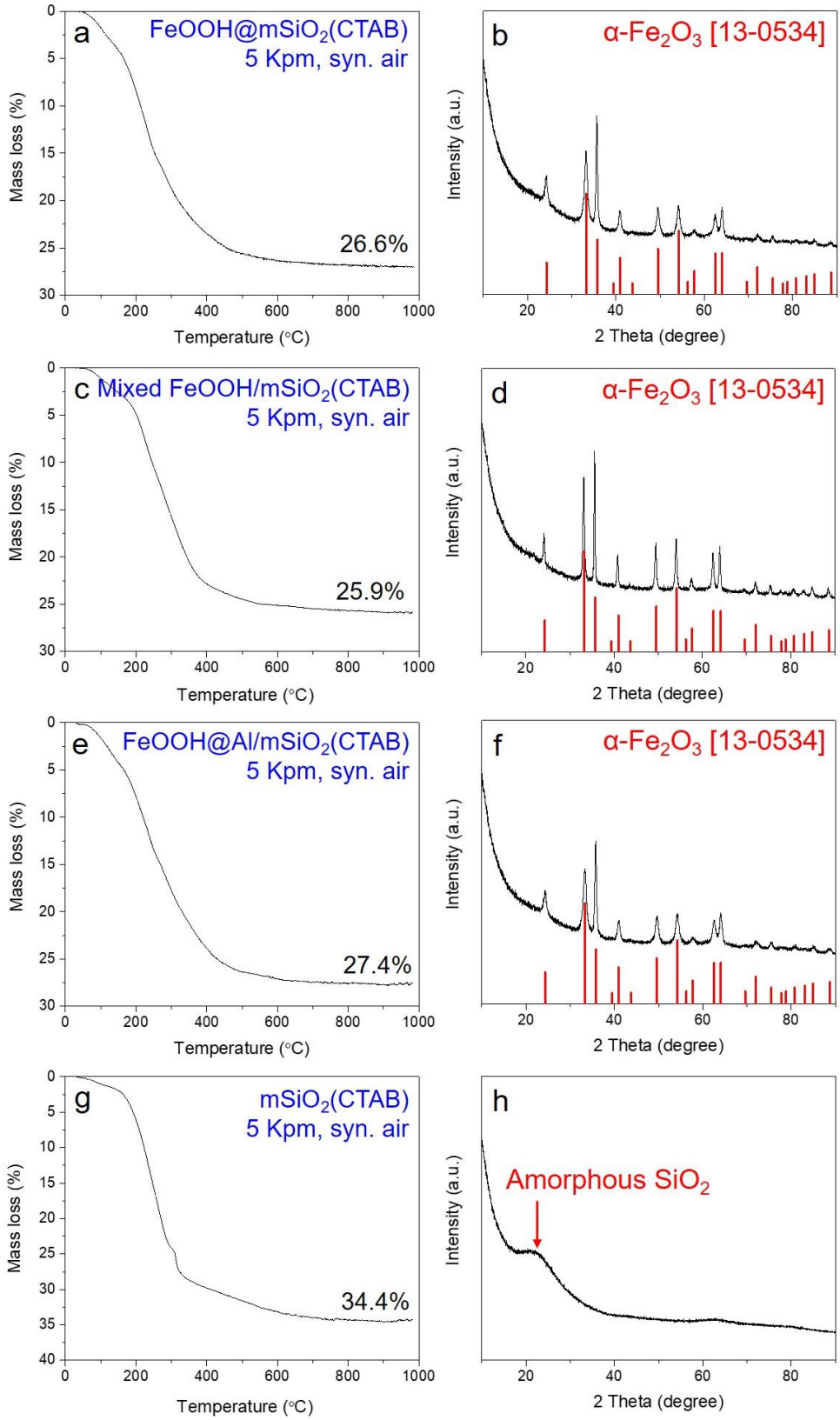

Figure S1. TG curves during calcination (in Air) and the corresponding XRD patterns after TG measurements of (a,b) FeOOH@$mSiO_2$(CTAB), (c,d) mixed FeOOH/$mSiO_2$(CTAB), (e,f) FeOOH@Al/$mSiO_2$(CTAB) and (g,h) $mSiO_2$(CTAB).

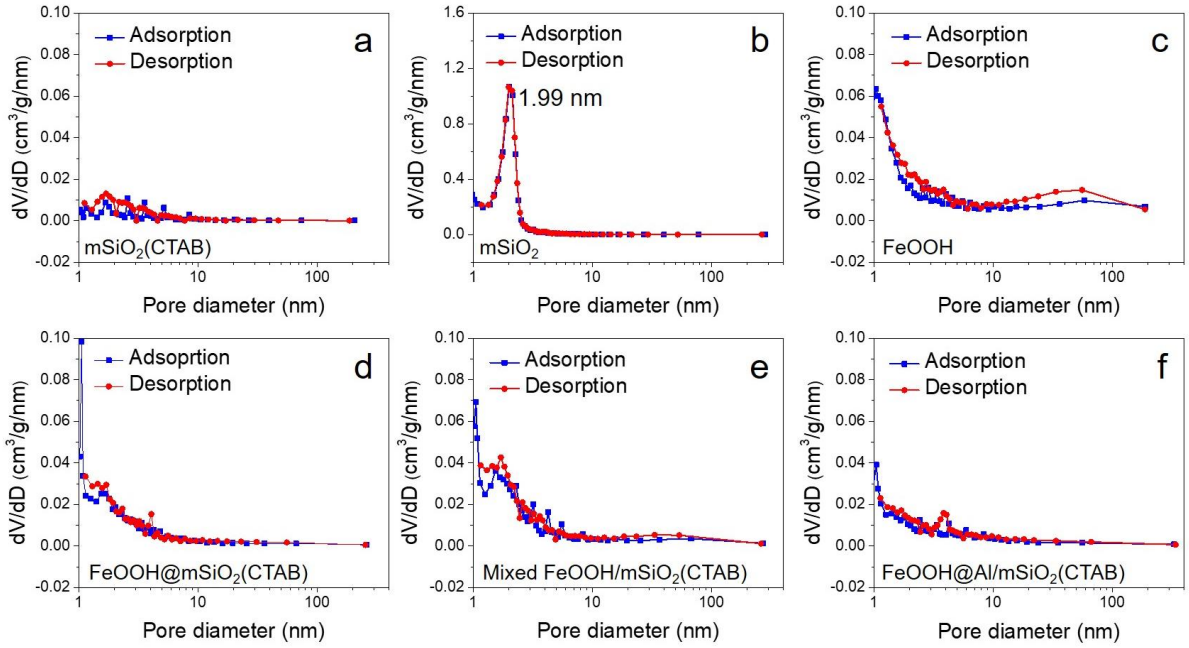

Figure S2. Pore size distribution curves of $mSiO_2$(CTAB) (a) before and (b) after calcination; (c) FeOOH nanosheets; (d) FeOOH@$mSiO_2$(CTAB); (e) Mixed FeOOH/$mSiO_2$(CTAB) and (f) FeOOH@Al/$mSiO_2$(CTAB).

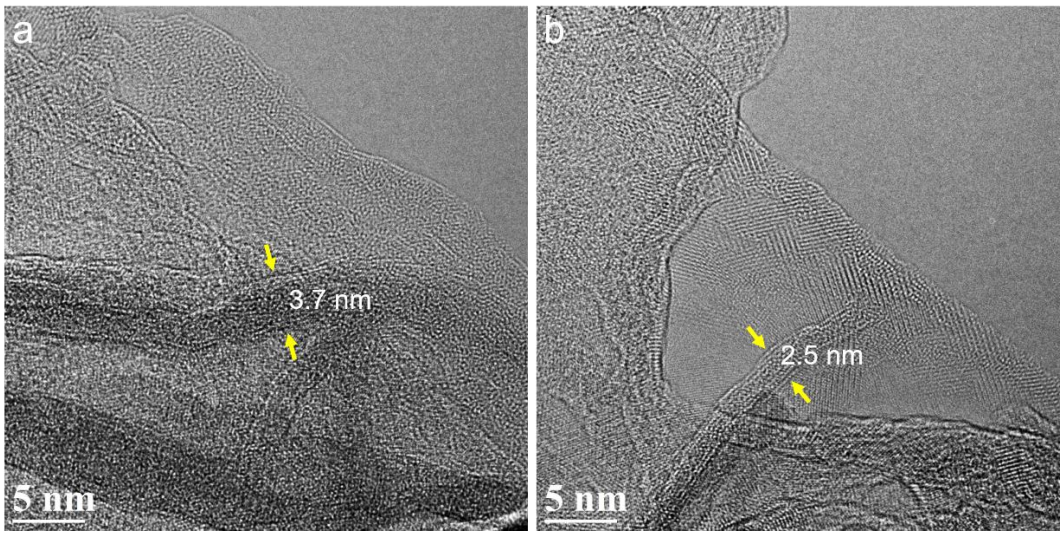

Figure S3. (a,b) HRTEM images of FeOOH nanosheets. The thickness of FeOOH nanosheets is measured as 2-4 nm.

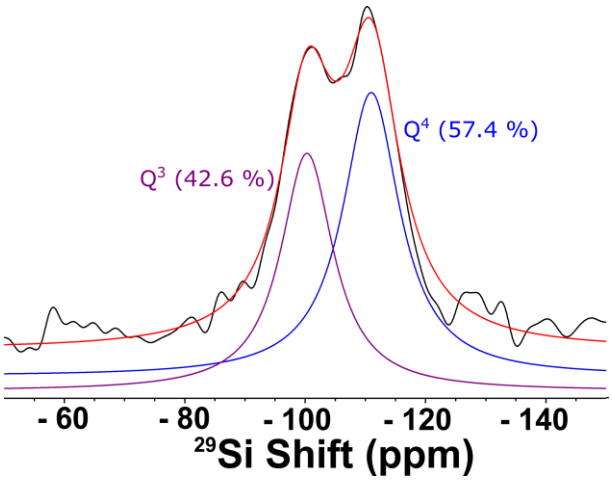

Figure S4. ^{29}Si MAS NMR spectrum of the coated sample without Al dopant.

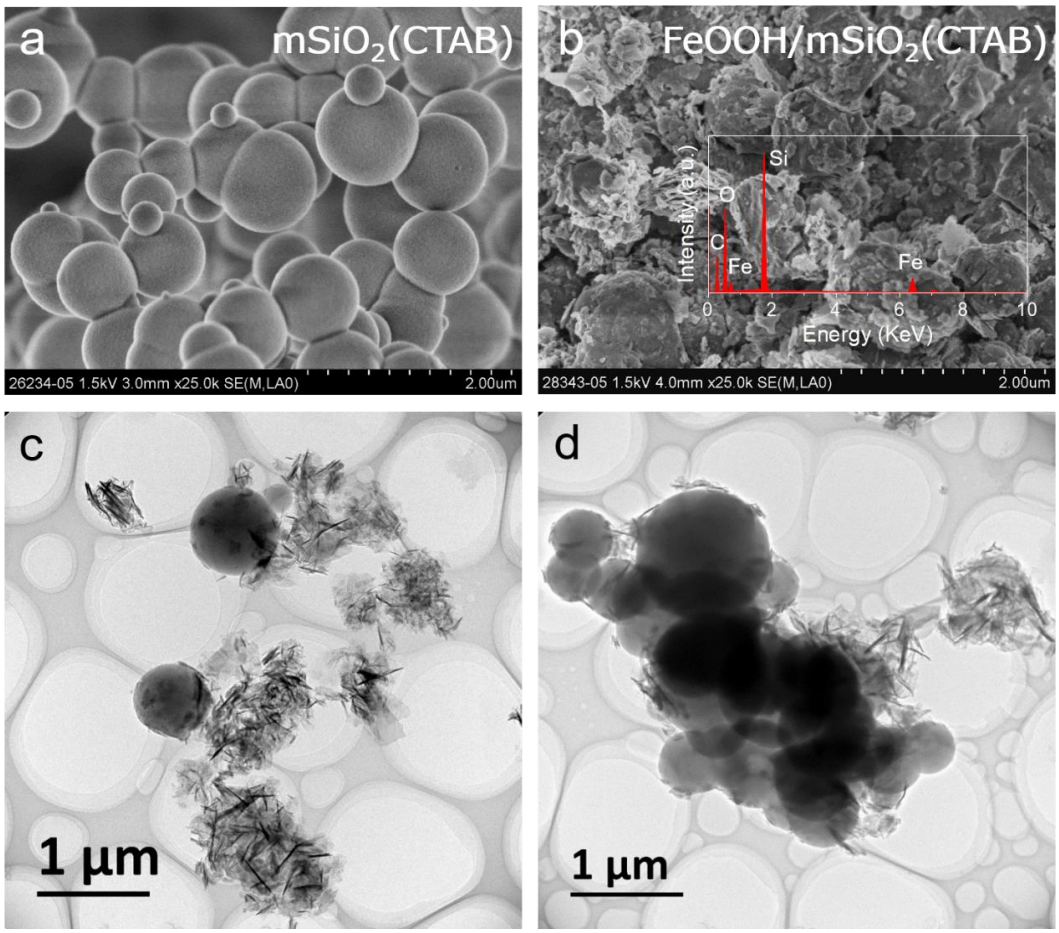

Figure S5. SEM images of (a) $mSiO_2$(CTAB) support and (b) mixed FeOOH/$mSiO_2$(CTAB); (c,d) TEM images of mixed FeOOH/$mSiO_2$(CTAB). Inset of (b) shows the corresponding EDX.

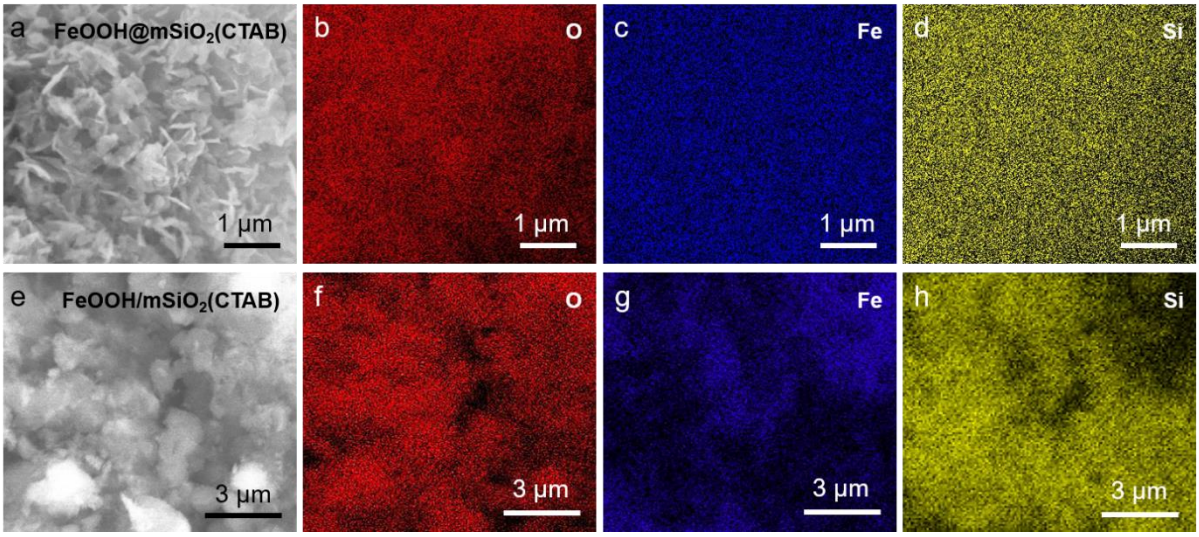

Figure S6. Low-magnification SEM images of (a) FeOOH@mSiO$_2$(CTAB) and (e) FeOOH/mSiO$_2$(CTAB); (b-d, f-h) the corresponding elemental maps of O, Fe and Si.

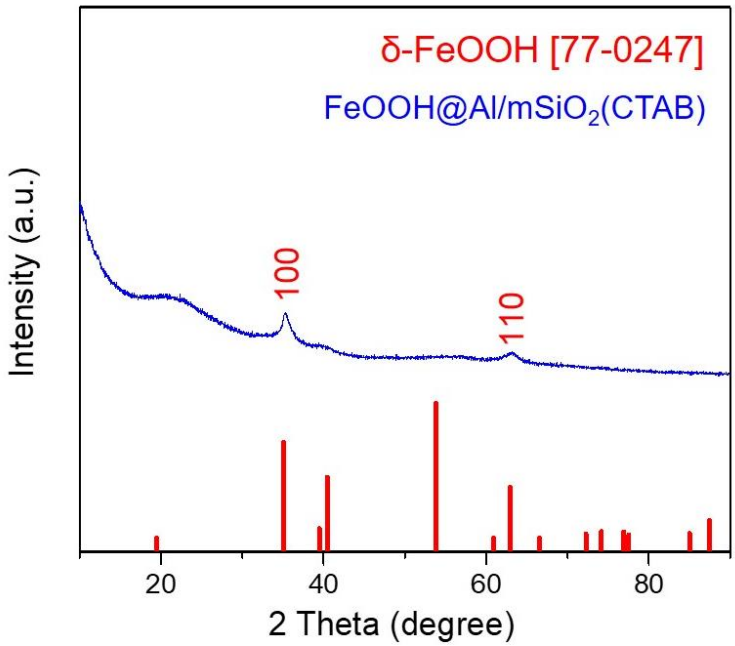

Figure S7. XRD pattern of the coated sample with Al dopant.

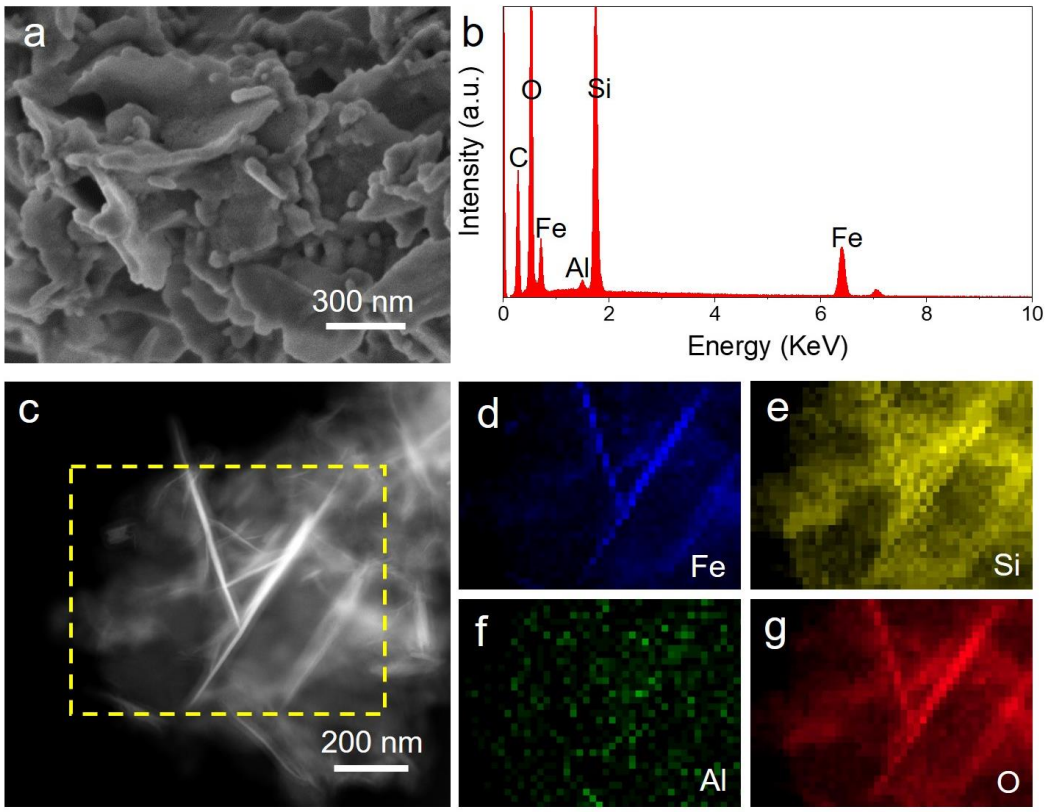

Figure S8. (a) SEM image, (c) HAADF-STEM image and (b, d-g) the corresponding elemental analysis of the coated sample with Al dopant.

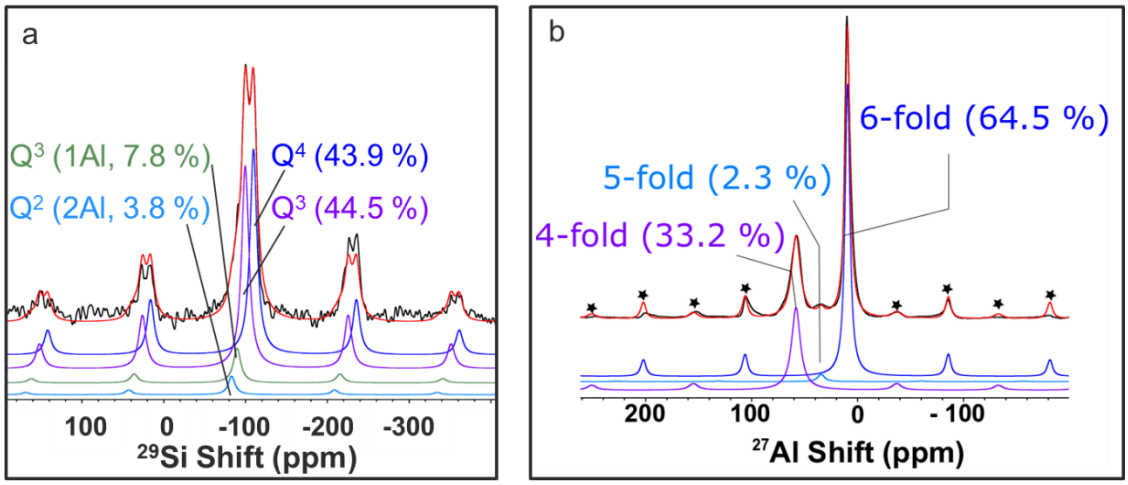

Figure S9. (a) ^{29}Si and (b) ^{27}Al MAS NMR spectra of the coated sample with Al dopant. Spinning sidebands are marked by asterisks.

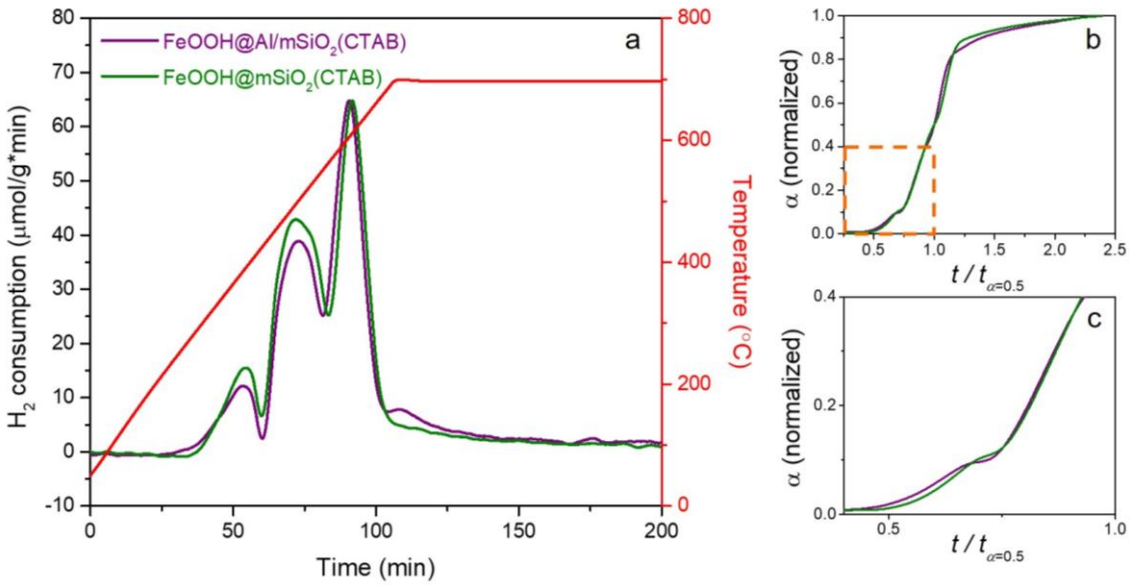

Figure S10. (a) H_2-TPR and (b,c) integrated TPR curves to time-fractions ($t/t_{\alpha=0.5}$) of the coated samples with (purple) and without (green) Al doping. Conditions: 5%H_2/Ar, 80 mL min^{-1}, 6 °C min^{-1}, 700 °C, 90 min holding time.

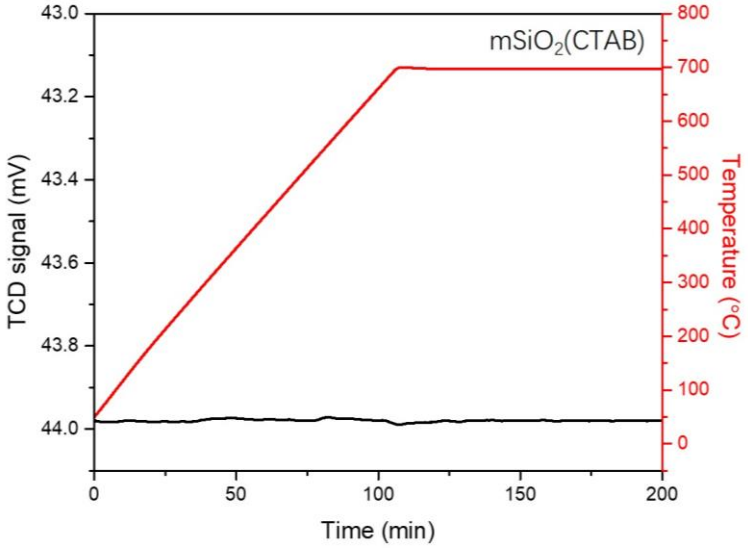

Figure S11. TPR profile of $mSiO_2$(CTAB), showing no obvious presence of H_2 consumption.

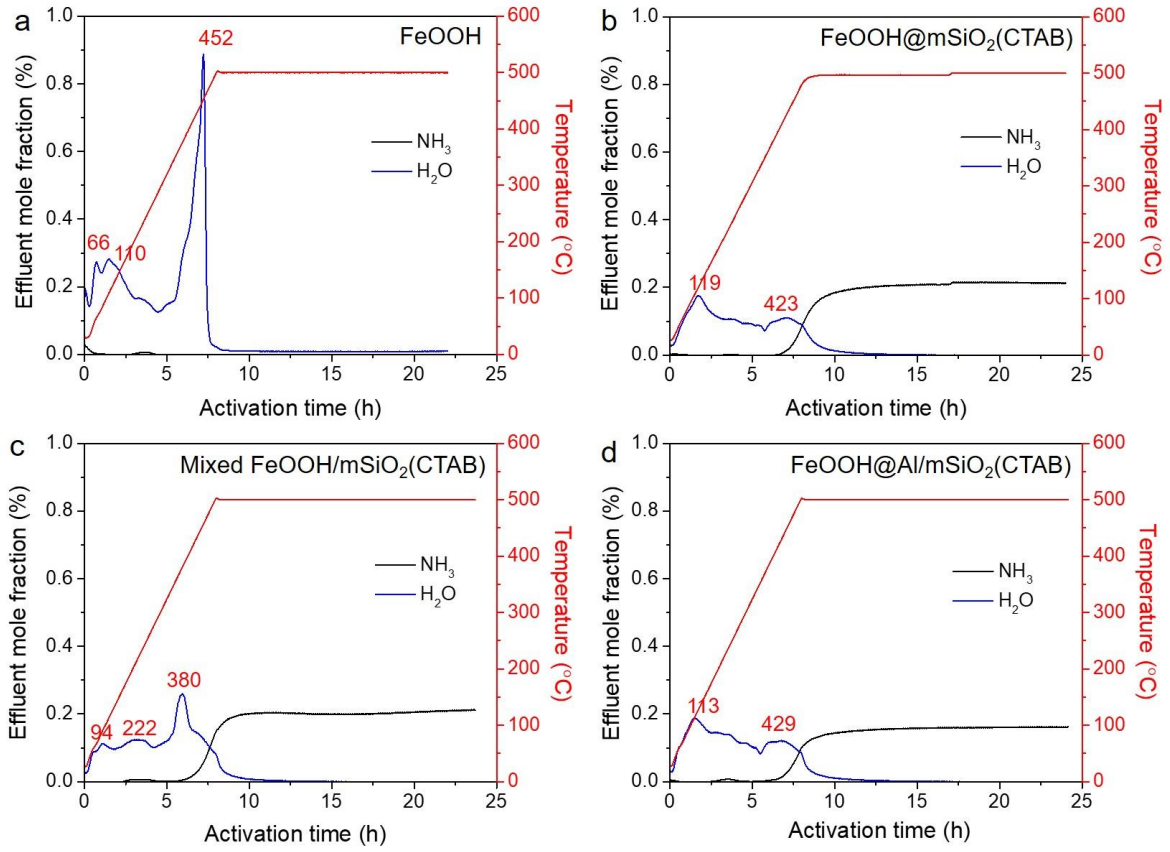

Figure S12. Time course of NH_3 and H_2O evolution during *in situ* activation. Activation conditions: 75%H_2/N_2, 440 NmL min^{-1}, 1 °C min^{-1}, 500 °C, 14-16 h holding time.

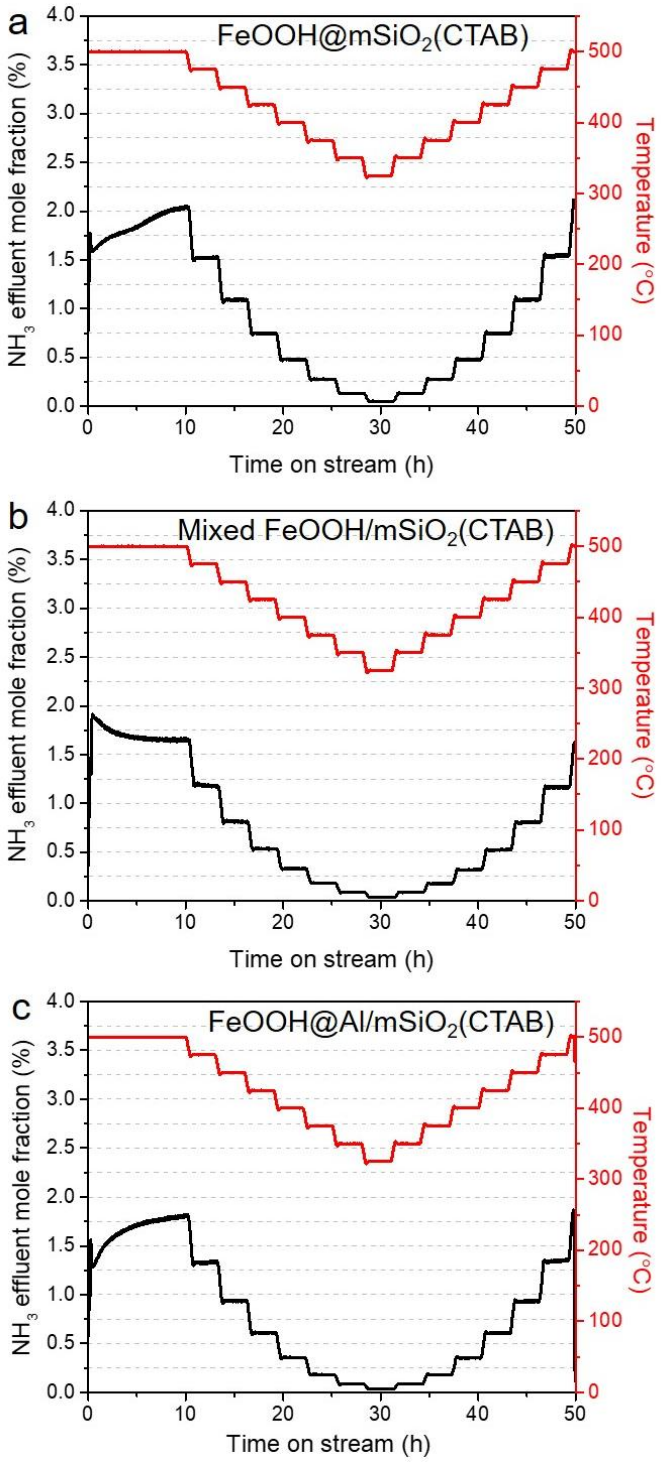

Figure S13. Ammonia effluent mole fraction at different temperatures. All temperatures were kept constant for 155 min.

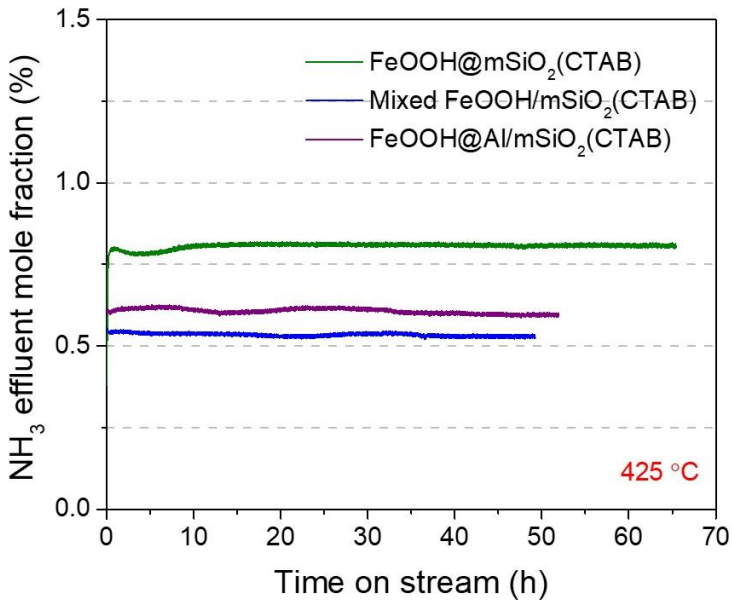

Figure S14. Stability tests on encapsulated and supported catalysts.

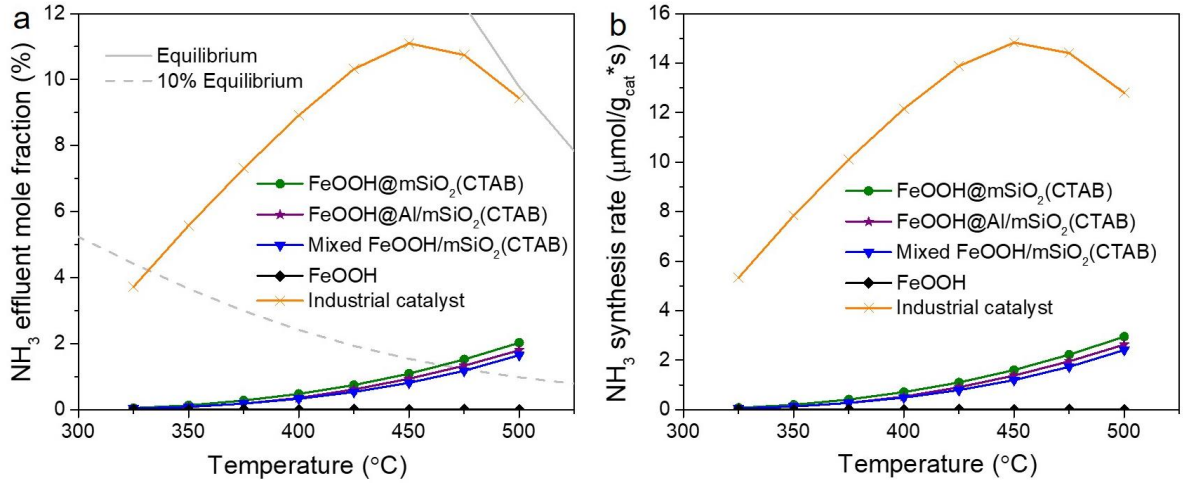

Figure S15. (a) Ammonia effluent mole fraction obtained in steady state at different temperatures under 90 bar; (b) Rate of ammonia synthesis normalized by catalyst mass.

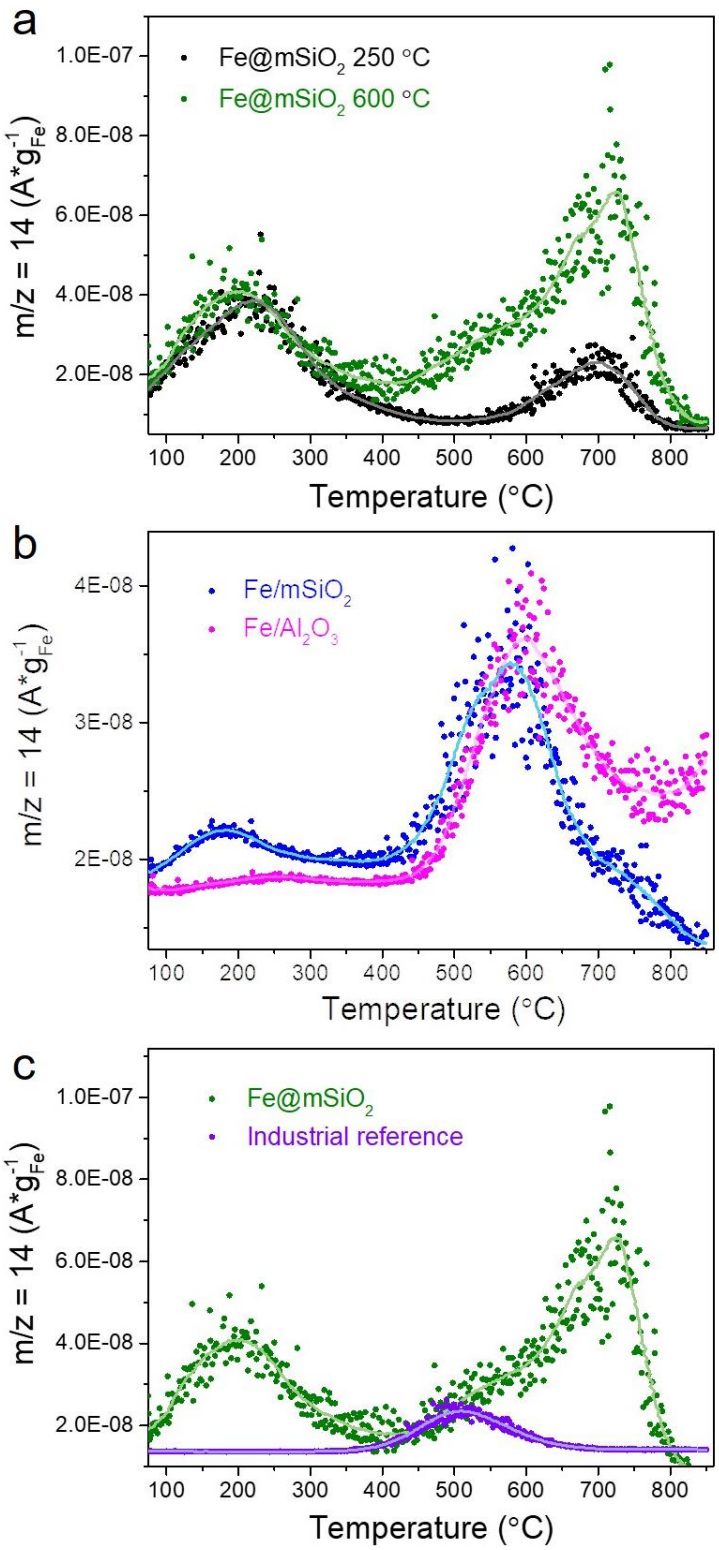

Figure S16. (a) TDS spectra of the $mSiO_2$ coated catalyst treated by 75%H_2/N_2 at 250 °C and 600 °C; Differences of the TDS spectra between (b) $mSiO_2$ supported and Al_2O_3 supported catalysts; (c) $mSiO_2$ coated catalyst and industrial catalyst.

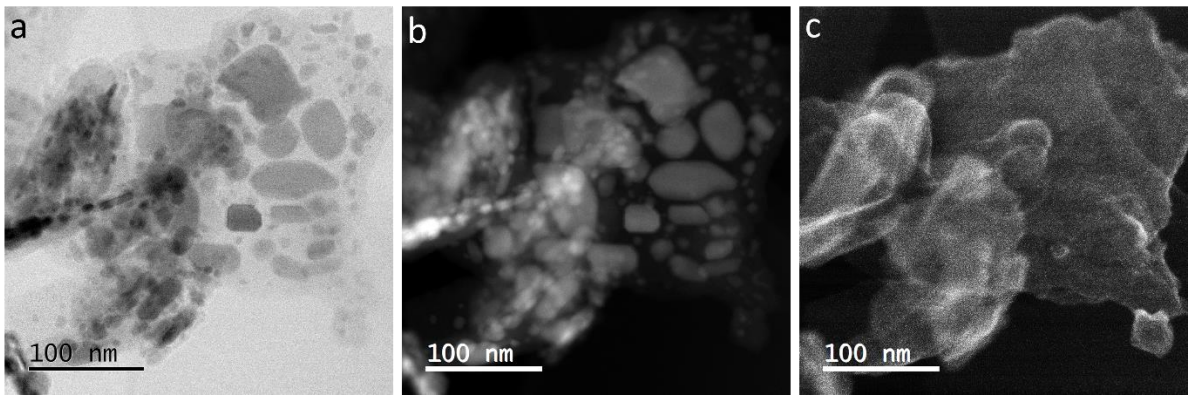

Figure S17. (a) ABF-STEM image, (b) HAADF-STEM image and (c) SE image of spent encapsulated catalyst.

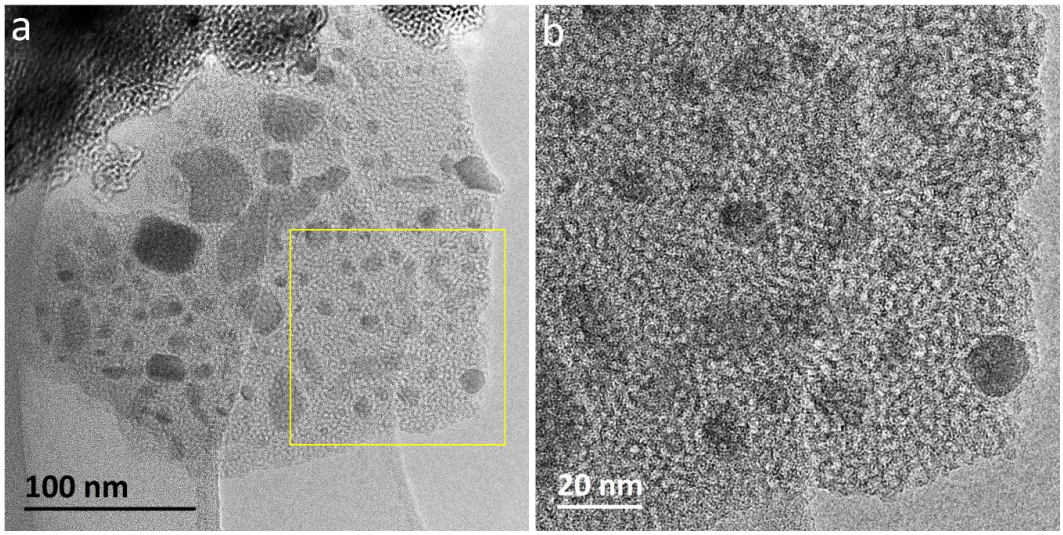

Figure S18. (a,b) TEM images of spent encapsulated catalyst, showing clearly the presence of pores in the capping SiO_2 layers.

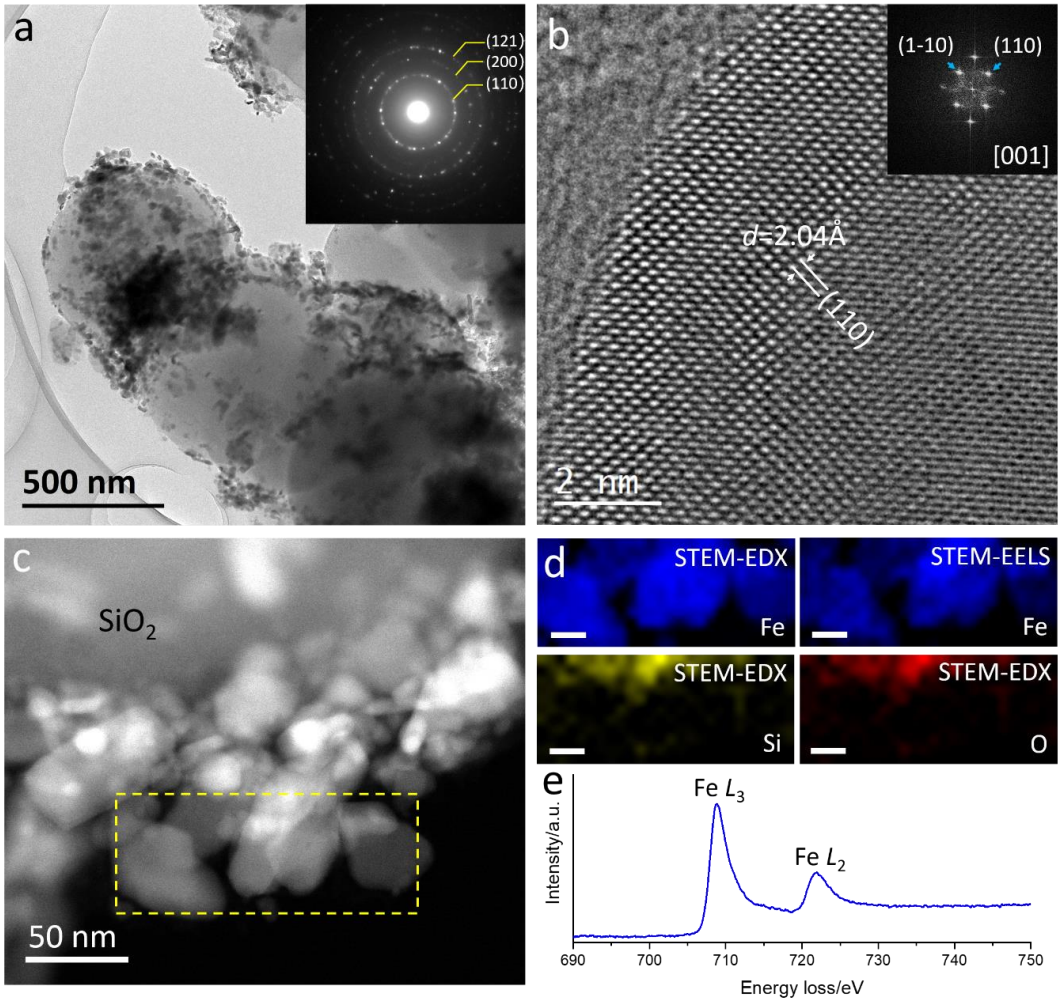

Figure S19. (a) TEM and (b) HRTEM images of supported Fe catalyst after catalytic reaction; Inset of (b) shows the SAED pattern of the sample; (c) HAADF-STEM image and (d) the corresponding STEM-EDX elemental maps of Fe, Si and O as well as STEM-EELS map of Fe and corresponding EELS spectrum; Scale bar in (d) is 20 nm.

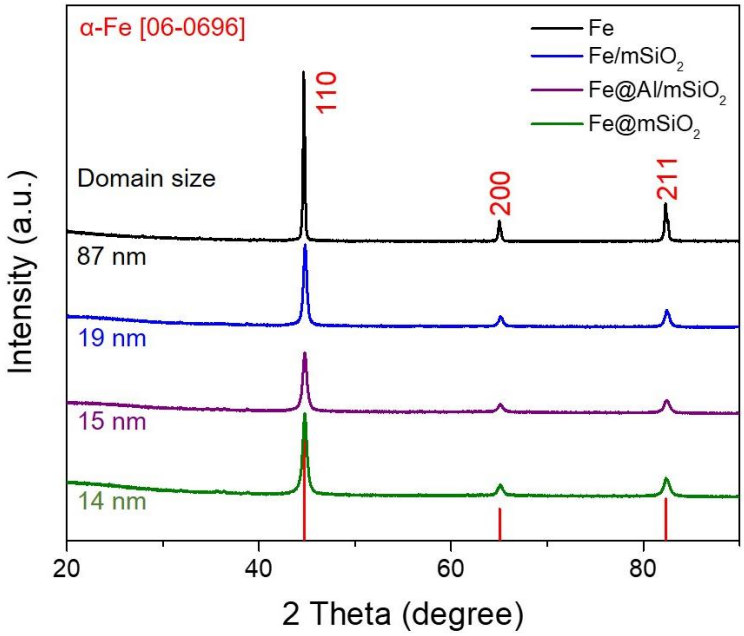

Figure S20. XRD patterns of the catalysts after NH_3 synthesis and the corresponding Fe domain sizes.

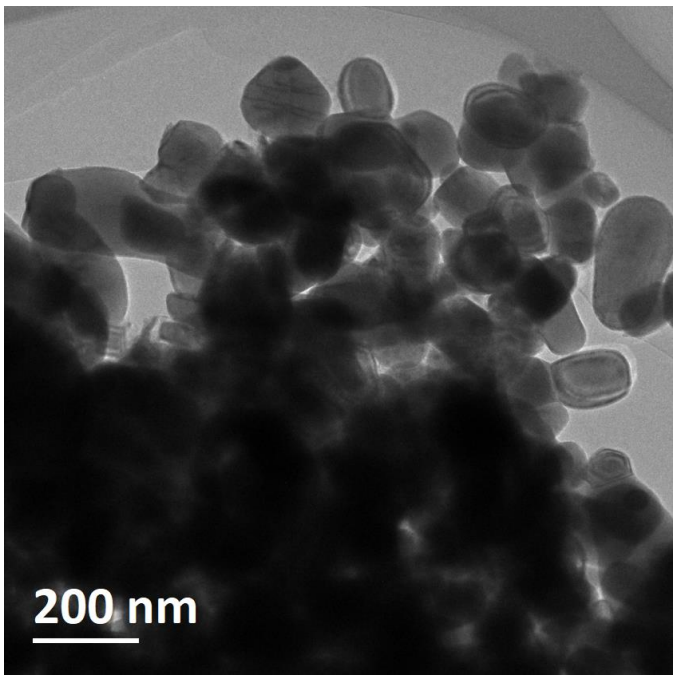

Figure S21. TEM images of the unsupported Fe catalyst after catalytic reaction.

REFERENCES

[1] R. Schlögl. Catalytic Synthesis of Ammonia—A “Never-Ending Story”? *Angew. Chem. Int. Ed.* **2003,** *42*, 2004-2008.

[2] J. W. Erisman, M. A. Sutton, J. Galloway, Z. Klimont,W. Winiwarter. How a century of ammonia synthesis changed the world. *Nat. Geosci.* **2008,** *1*, 636-639.

[3] R. Schlögl. Ammonia Synthesis. In *Handbook of Heterogeneous Catalysis*; Wiley-VCH Verlag GmbH & Co. KGaA: 2008.

[4] M. Appl. Ammonia, 1. Introduction. In *Ullmann's Encyclopedia of Industrial Chemistry*; Wiley-VCH Verlag GmbH & Co. KGaA: 2000.

[5] A. Klerke, C. H. Christensen, J. K. Norskov,T. Vegge. Ammonia for hydrogen storage: challenges and opportunities. *J. Mater. Chem.* **2008,** *18*, 2304-2310.

[6] F. Schuth, R. Palkovits, R. Schlogl,D. S. Su. Ammonia as a possible element in an energy infrastructure: catalysts for ammonia decomposition. *Energy Environ. Sci.* **2012,** *5*, 6278-6289.

[7] S. Mitsushima,V. Hacker. Chapter 11 - Role of Hydrogen Energy Carriers. In *Fuel Cells and Hydrogen*; Hacker, V.; Mitsushima, S., Eds.; Elsevier: 2018, pp 243-255.

[8] Y. Kojima. Hydrogen storage materials for hydrogen and energy carriers. *Int. J. Hydrogen Energy* **2019,** *44*, 18179-18192.

[9] K. E. Lamb, M. D. Dolan,D. F. Kennedy. Ammonia for hydrogen storage; A review of catalytic ammonia decomposition and hydrogen separation and purification. *Int. J. Hydrogen Energy* **2019,** *44*, 3580-3593.

[10] M. Appl. Ammonia, 2. Production Processes. In *Ullmann's Encyclopedia of Industrial Chemistry*; Wiley-VCH Verlag GmbH & Co. KGaA: 2000.

[11] S. Licht, B. Cui, B. Wang, F.-F. Li, J. Lau,S. Liu. Ammonia synthesis by N_2 and steam electrolysis in molten hydroxide suspensions of nanoscale Fe_2O_3. *Science* **2014,** *345*, 637.

[12] Y. Zhao, R. Shi, X. Bian, C. Zhou, Y. Zhao, S. Zhang, F. Wu, G. I. N. Waterhouse, L.-Z. Wu, C.-H. Tung,T. Zhang. Ammonia Detection Methods in Photocatalytic and Electrocatalytic Experiments: How to Improve the Reliability of NH_3 Production Rates? *Adv. Sci.* **2019,** *6*, 1802109.

[13] Sustainable Ammonia Synthesis—Exploring the scientific challenges associated with discovering alternative, sustainable processes for ammonia production. DOE Roundtable Report; US Department of Energy, Office of Science: Dulles, VA, 2016; https://science.energy.gov/~/media/bes/pdf/reports/2016/SustainableAmmoniaReport.pdf.

[14] T. Kandemir, M. E. Schuster, A. Senyshyn, M. Behrens,R. Schlögl. The Haber–Bosch Process Revisited: On the Real Structure and Stability of “Ammonia Iron” under Working Conditions. *Angew. Chem. Int. Ed.* **2013,** *52*, 12723-12726.

[15] N. D. Spencer, R. C. Schoonmaker,G. A. Somorjai. Structure sensitivity in the iron single-crystal catalysed synthesis of ammonia. *Nature* **1981,** *294*, 643-644.

[16] G. A. Somorjai,N. Materer. Surface structures in ammonia synthesis. *Top. Catal.* **1994,** *1*, 215-231.

[17] J. J. Mortensen, M. V. Ganduglia-Pirovano, L. B. Hansen, B. Hammer, P. Stoltze,J. K. Nørskov. Nitrogen adsorption on Fe(111), (100), and (110) surfaces. *Surf. Sci.* **1999,** *422*, 8-16.

[18] J. A. Dumesic, H. Topsøe, S. Khammouma,M. Boudart. Surface, catalytic and magnetic properties of small iron particles: II. Structure sensitivity of ammonia synthesis. *J. Catal.* **1975,** *37*, 503-512.

[19] S. Dahl, A. Logadottir, R. C. Egeberg, J. H. Larsen, I. Chorkendorff, E. Törnqvist,J. K. Nørskov. Role of Steps in N_2 Activation on Ru(0001). *Phys. Rev. Lett.* **1999,** *83*, 1814-1817.

[20] R. C. Egeberg, S. Dahl, A. Logadottir, J. H. Larsen, J. K. Nørskov,I. Chorkendorff. N_2 dissociation on Fe(110) and Fe/Ru(0001): what is the role of steps? *Surf. Sci.* **2001,** *491*, 183-194.

[21] J. K. Norskov, T. Bligaard, B. Hvolbaek, F. Abild-Pedersen, I. Chorkendorff,C. H. Christensen. The nature of the active site in heterogeneous metal catalysis. *Chem. Soc. Rev.* **2008,** *37*, 2163-2171.

[22] P. Ding, F. Luo, P. Wang, W. Xia, X. Xu, J. Hu,H. Zeng. Photo-induced charge kinetic acceleration in ultrathin layered double hydroxide nanosheets boosts the oxygen evolution reaction. *J. Mater. Chem. A* **2020**.

[23] X. Zhang, T. Wu, H. Wang, R. Zhao, H. Chen, T. Wang, P. Wei, Y. Luo, Y. Zhang,X. Sun. Boron Nanosheet: An Elemental Two-Dimensional (2D) Material for Ambient Electrocatalytic N_2-to-NH_3 Fixation in Neutral Media. *ACS Catal.* **2019,** *9*, 4609-4615.

[24] Y. Zhu, L. Peng, Z. Fang, C. Yan, X. Zhang,G. Yu. Structural Engineering of 2D Nanomaterials for Energy Storage and Catalysis. *Adv. Mater.* **2018,** *30*, 1706347.

[25] D. Deng, K. S. Novoselov, Q. Fu, N. Zheng, Z. Tian,X. Bao. Catalysis with two-dimensional materials and their heterostructures. *Nat. Nanotechnol.* **2016,** *11*, 218-230.

[26] H. Yin,Z. Tang. Ultrathin two-dimensional layered metal hydroxides: an emerging platform for advanced catalysis, energy conversion and storage. *Chem. Soc. Rev.* **2016,** *45*, 4873-4891.

[27] Y. Sun, S. Gao, F. Lei,Y. Xie. Atomically-thin two-dimensional sheets for understanding active sites in catalysis. *Chem. Soc. Rev.* **2015,** *44*, 623-636.

[28] S. Bai,Y. Xiong. Recent Advances in Two-Dimensional Nanostructures for Catalysis Applications. *Sci. Adv. Mater.* **2015,** *7*, 2168-2181.

[29] H. Fan, X. Huang, L. Shang, Y. Cao, Y. Zhao, L.-Z. Wu, C.-H. Tung, Y. Yin,T. Zhang. Controllable Synthesis of Ultrathin Transition-Metal Hydroxide Nanosheets and their Extended Composite Nanostructures for Enhanced Catalytic Activity in the Heck Reaction. *Angew. Chem. Int. Ed.* **2016,** *55*, 2167-2170.

[30] H. Fan, X. Huang, K. Kähler, J. Folke, F. Girgsdies, D. Teschner, Y. Ding, K. Hermann, R. Schlögl,E. Frei. In-Situ Formation of Fe Nanoparticles from FeOOH Nanosheets on γ-Al_2O_3 as Efficient Catalysts for Ammonia Synthesis. *ACS Sustain. Chem. Eng.* **2017,** *5*, 10900-10909.

[31] L. Shang, T. Bian, B. Zhang, D. Zhang, L.-Z. Wu, C.-H. Tung, Y. Yin,T. Zhang. Graphene-Supported Ultrafine Metal Nanoparticles Encapsulated by Mesoporous Silica: Robust Catalysts for Oxidation and Reduction Reactions. *Angew. Chem. Int. Ed.* **2014,** *53*, 250-254.

[32] W. Li,D. Zhao. Extension of the Stöber Method to Construct Mesoporous SiO_2 and TiO_2 Shells for Uniform Multifunctional Core–Shell Structures. *Adv. Mater.* **2013,** *25*, 142-149.

[33] Z. Teng, G. Zheng, Y. Dou, W. Li, C.-Y. Mou, X. Zhang, A. M. Asiri,D. Zhao. Highly Ordered Mesoporous Silica Films with Perpendicular Mesochannels by a Simple Stöber-Solution Growth Approach. *Angew. Chem. Int. Ed.* **2012,** *51*, 2173-2177.

[34] P. Chen, K. Xu, X. Li, Y. Guo, D. Zhou, J. Zhao, X. Wu, C. Wu,Y. Xie. Ultrathin nanosheets of feroxyhyte: a new two-dimensional material with robust ferromagnetic behavior. *Chem. Sci.* **2014,** *5*, 2251-2255.

[35] H. L. Ding, Y. X. Zhang, S. Wang, J. M. Xu, S. C. Xu,G. H. Li. Fe_3O_4@SiO_2 Core/Shell Nanoparticles: The Silica Coating Regulations with a Single Core for Different Core Sizes and Shell Thicknesses. *Chem. Mater.* **2012,** *24*, 4572-4580.

[36] D. Zhao, Y. Wang,W. Zhou. Structural Characterization Methods. In *Ordered Mesoporous Materials*; 2013, pp 117-151.

[37] D. Zhao, Y. Wang,W. Zhou. Doping in Mesoporous Molecular Sieves. In *Ordered Mesoporous Materials*; 2013, pp 219-242.

[38] L. V. C. Lima, M. Rodriguez, V. A. A. Freitas, T. E. Souza, A. E. H. Machado, A. O. T. Patrocínio, J. D. Fabris, L. C. A. Oliveira,M. C. Pereira. Synergism between n-type WO_3 and p-type δ-FeOOH semiconductors: High interfacial contacts and enhanced photocatalysis. *Appl. Catal. B: Environ* **2015,** *165*, 579-588.

[39] S. Zhang, Y. Tang, L. Nguyen, Y.-F. Zhao, Z. Wu, T.-W. Goh, J. J. Liu, Y. Li, T. Zhu, W. Huang, A. I. Frenkel, J. Li,F. F. Tao. Catalysis on Singly Dispersed Rh Atoms Anchored on an Inert Support. *ACS Catal.* **2018,** *8*, 110-121.

[40] C. E. Lovell, J. Scott,R. Amal. Ni-SiO2 Catalysts for the Carbon Dioxide Reforming of Methane: Varying Support Properties by Flame Spray Pyrolysis. *Molecules* **2015,** *20*.

[41] Q. G. Zhu, H. Iwasaki, E. D. Williams,R. L. Park. Formation of iron silicide thin films. *J. Appl. Phys.* **1986,** *60*, 2629-2631.

[42] X. Huang, D. Teschner, M. Dimitrakopoulou, A. Fedorov, B. Frank, R. Kraehnert, F. Rosowski, H. Kaiser, S. Schunk, C. Kuretschka, R. Schlögl, M.-G. Willinger,A. Trunschke. Inside Cover: Atomic-Scale Observation of the Metal–Promoter Interaction in Rh-Based Syngas-Upgrading Catalysts (Angew. Chem. Int. Ed. 26/2019). *Angew. Chem. Int. Ed.* **2019,** *58*, 8596-8596.

[43] H. Tan, J. Verbeeck, A. Abakumov,G. Van Tendeloo. Oxidation state and chemical shift investigation in transition metal oxides by EELS. *Ultramicroscopy* **2012,** *116*, 24-33.